UNIVERSITY OF COPENHAGEN
FACULTY OF SCIENCE

UNIVERSITY OF COPENHAGEN

Masters Thesis

Environmentally induced neutrino decoherence in IceCube

Mikkel Jensen

Advisors: Dr. David Jason Koskinen and Dr. Thomas Simon Stuttard

Submitted: July 24, 2018

Abstract

Neutrino oscillations were discovered two decades ago and the theory have since been able to describe neutrino data accurately. The increase in detector capabilities coming with advances in technology delivers oscillation parameter measurements with increasing precision, which requires analyses of potential sub-leading effects to ensure that the data is not misinterpreted.

Quantum decoherence of neutrinos has the potential to be such an effect, and is motivated by certain quantum gravity models. It acts as a damping effect on neutrino oscillation probabilities. In decoherence theory the neutrinos are coupled to the environment, in which they propagate. This coupling can be described by a parameter, Γ, that characterizes the frequency and magnitude of perturbations caused by "interactions" with the environment. The coupling could depend on the neutrino energy, and models where the energy dependence follows a power law with $\Gamma = \Gamma_0 \left(\frac{E_\nu}{GeV}\right)^n$ are investigated in this thesis.

The existence of decoherence can be detected or limited by using the IceCube detector located at the geographic South Pole. IceCube is one of the best detectors for probing decoherence effects, due to the many different distances neutrinos generated in the Earth's atmosphere travel before detection. The potential to discover decoherence is calculated by using pseudodata. IceCube has an expected sensitivity down to $\Gamma = 1.6$ *feV* at 90% confidence, when considering the energy independent decoherence case.

Acknowledgments

The time that i have spent in the past year and a half with the IceCube group has been both enlightening and demanding. I am happy that Jason allowed me to be introduced to the world of experimental neutrino physics, despite my (at that time) complete lack of coding skills. The introduction to programming and advanced statistics has been both exciting and beneficial, a statement which i would never have thought to be true a couple of years back.

I would like to thank everyone in the IceCube group for always taking the time to help out, and for their willingness to explain the same thing multiple times when needed. This includes the people in the office, Etienne, Michael, and Tom, but also Morten and of course Jason. Furthermore i would like to thank Markus for explaining and discussing the parts of density matrix and decoherence theory, whenever my understanding fell short.

I think it is in order to applaud Tom additionally for his part in this project, and his knowledge about everything related to the analysis. You have been able to explain almost everything i did not understand or did not had prior knowledge of. This project would not have come very far without your contributions.

I am grateful that my Mom and Dad always ask about how my studies are going, and pay an interest in what i am doing. You have always supported me in getting educated, and definitely have a part in me coming this far.

Last but not least i would like to thank my girlfriend Josefine, who is always supporting me in (almost) everything i am doing. Especially in the final weeks where i have not had a lot of spare time. You have been able to make my life easier by having dinner ready when i got home, and have backed me in working in the weekends in order to finish the project.

Author's contributions

This work includes implementation and testing of a neutrino decoherence model, and an IceCube related analysis of the estimated limits to detection. I joined the IceCube group around the beginning of 2017 and intended to do a search for magnetic monopoles. The search was more complex than first thought, and the project was changed. Much of the work related to neutrino decoherence has been done in cooperation with Dr. Thomas Simon Stuttard. For that reason my main contributions are highlighted here.

I have tested the accuracy and speed of different oscillation probability calculators to determine which was the best for implementing neutrino decoherence. A decoherence toy model which is used in section 4.1 was created by me to better understand how contact with a surrounding environment affects the propagation of neutrinos. I have been a part of implementing a decoherence model in IceCube sofware. That part of the work includes an implementation of bounds on the values that three decoherence parameters can take, which depends on each of their individual values, as well as exploration of how distinguishable different decoherence models are in IceCube, and limits for detecting a signal.

I have also added an energy dependent decoherence model in which the strength follows a power law $\propto E^n$, where the cases $n \in [-2, -1, 0, 1, 2]$ are investigated. This allows for the sensitivity to decoherence that depends on neutrino energy to be estimated. Energy dependent decoherence is addressed in section 4.2.1 and 5.8.1.

Contents

List of Figures

List of Tables

Introduction

1

This work includes the description of a theory of neutrinos propagating in an environment to which they are coupled, and how this leads to an effect known as decoherence. A prerequisite for this has been the understanding of how particles can be described with a density matrix formalism. The decoherence effect can be defined by the three parameters Γ_{21}, Γ_{31}, and Γ_{32}, which arise from the Lindblad equation.

Neutrino oscillations are revisited in the decoherence framework, which required investigation of various topics including the impact on oscillations, degeneracy of parameters, bounds on decoherence parameter space, implementation in software, and dependence on energy.

The original motivation for the project was a tension in results from two separate neutrino accelerator experiments, which could potentially be explained with decoherence. The tension has been resolved since, but decoherence remains interesting as a probe for certain quantum gravity models, which predicts the effect.

1.1 Brief history of neutrinos

Neutrinos were originally proposed by Wolfgang Pauli in 1930 [1] to explain why the energies of electrons produced in β-decay were distributed over a range, rather than having a single value, as expected in a two body decay due to conservation of energy. This could be explained by characterizing β-decay as a three body problem. The electron energies would then vary depending on how much of the energy went to the momentum of the third particle. This new particle had to be neutral to conserve charge in the β-decay.

The neutrino wasn't experimentally confirmed until 26 years later, when Cowan and Reines detected the antielectron neutrino via inverse β-decay $\bar{\nu}_e + p \rightarrow n + e^+$ [2]. In the experiment, an antielectron neutrino interacts with a proton in a mixture of water and cadmium chloride to create a neutron and a positron. The positron annihilates with an electron in the medium shortly after creation and emits two γ-rays. After a delay, the neutron is captured in cadmium, releasing more γ-rays. The neutrino is then detected indirectly by observing this delayed light signature.

During the 1960's the solar neutrino problem arose from results of the Homestake experiment [3]. This experiment was only sensitive to the neutrino flavor created in the sun, namely electron neutrinos. The neutrino flux observed at Homestake was about 1/3 of the expected flux predicted by solar fusion models. Neutrino oscillations were proposed as a solution to the problem, but were not confirmed until the early 2000's by the Sudbury Neutrino Observatory (SNO) and Super Kamiokande experiments. This explained the deficit in flux and resolved the issue. The neutrinos had changed flavor along the way of propagation through oscillations. The Nobel prize in physics was awarded to Arthur B. McDonald and Takaaki Kajita in 2015 for the discovery of neutrino oscillations.

1.2 Neutrinos and the Standard model

The Standard Model in physics has been widely successful in its predictions and descriptions of elementary particle physics. It contains the description of three fundamental forces; electromagnetic, weak, and strong nuclear force, and how elementary particles interact via these. One of the many reasons why the Standard Model has been so successful is its predictive ability. Many of the known particles were theorized by the Standard Model prior to their discovery, which enhances its credibility. One of the only deviations observed so far is the fact that neutrinos are not massless, as predicted in the model. Neutrinos are now known to oscillate, which is not possible if they were massless.

The Standard Model particles displayed on figure 1.1, are grouped into two subgroups called fermions and bosons. The fermions are spin-half particles and come in three generations ranked from light to heavy. They are divided into two additional groups called quarks and leptons. Quarks come in six different flavors, and are the constituents of hadrons, such as protons, neutrons, and pions. Quark interactions occur via all fundamental forces. The leptons include both charged and neutral particles. Charged leptons interact electromagnetically, weakly, and gravitationally. Combined with baryons, the lightest charged lepton, the electron, make up most of the visible matter in the universe.

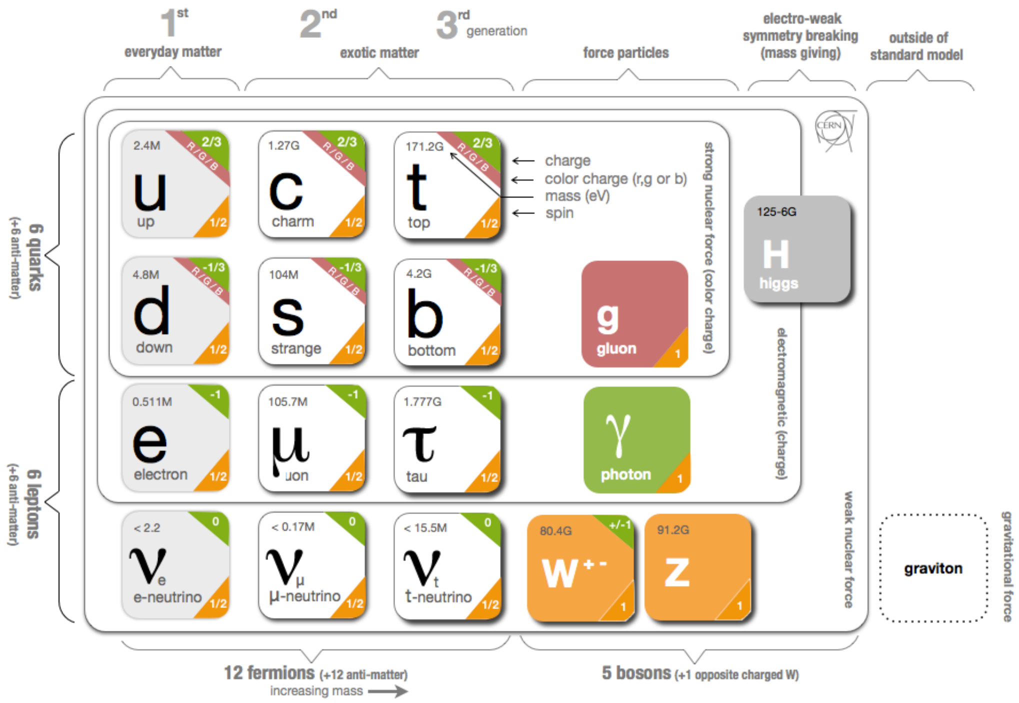

Figure 1.1. – Visualization of the Standard Model of particle physics. Taken from [4]

Neutral leptons, also called neutrinos, only interact weakly and gravitationally. Neutrinos are the second most abundant particle in the universe, only outnumbered by photons. They are extremely hard to detect due to the weakness of the weak force and their small mass.

Bosons on the other hand, are particles of integer spin. The gauge bosons (all bosons except the Higgs) mediate the force between interacting particles. Each force has its own force carrier(s). The strong nuclear force is mediated by gluons, and has the strongest coupling constant of all fundamental force, hence the name. The strength of the force increases with distance, as opposed to the other forces. For this reason quarks can never be observed alone. At large enough distances it is simply energetically favorable to create a new pair of quarks instead of further increasing the force. This phenomenon is also know as color confinement.

The weak nuclear force includes a charged current and a neutral current interaction. The mediators are massive with $m_W \sim 81 GeV$ and $m_Z \sim 90 GeV$ [5]. Weak interactions are caused by an exchange of a W or Z boson, which have extremely short lifetimes, under 10^{-24} seconds. This limits the range of the force to subatomic scales.

Photons are the carriers of electromagnetic force. Unlike the nuclear forces electromagnetism has a macroscopic range, which makes it important at all scales in the presence of charge. All charged particles can interact electromagnetically.

1.2.1 Beyond the Standard Model

There are still a variety of phenomena that can not be explained by the Standard Model. Gravitational attraction is not included, which is hypothesized to be governed by a particle called the graviton. It would be an intuitive extension to the Standard Model, since every other force can be described by the exchange of a particle. However, the scenario where some other mechanism would govern gravitational attraction is also plausible. Dark matter has been observed indirectly, by looking at the motion galaxies in galaxy clusters. The galaxies are moving at velocities that are greater than expected from gravitational attraction caused by the visible matter [6]. This is explained by attributing the excess in gravitational pull to a "dark" particle, that does not interact with electromagnetic radiation. There is no particle in the Standard Model that could explain what the dark matter observed in the universe consists of. Neutrinos are the only particles that do not interact with photons, but they do not fit the observed properties of dark matter. Dark energy is an even bigger mystery, and there is currently no evidence for what causes the accelerated expansion of the universe.

2 Neutrino oscillations

With the experimentally established fact that neutrinos oscillate [7], a theory is required to explain how the effect appears. This section covers the basic parts of neutrino oscillations theory. Neutrinos have a mismatch between flavor eigenstates in which they interact, and the mass eigenstates in which they propagate, meaning that each neutrino flavor eigenstate is a superposition of the mass eigenstates and vice versa. It will be shown how this mixing gives rise to a time-dependent oscillatory term in the equation for neutrino propagation. An introduction to density matrices is also needed in order to more easily understand and describe open quantum systems, which will be of interest later in this work.

2.1 Density matrix formalism

Usually, the wave function is used when describing a quantum system. This is sufficient when solving quantum systems in a pure state, i.e described by a single wave function. The density matrix formalism can be used to describe mixed states, which are statistical ensembles of pure states. They can describe quantum systems where the properties of the individual state is unknown, but the probability of being in each state is known. Throughout this work neutrino mass eigenstates will have a Latin subscript i, j, k etc. and flavor eigenstates a Greek subscript α, β, γ etc.

The density matrix for a pure state [8] is given by

$$\rho \quad = \quad |\psi\rangle \langle\psi| \,. \tag{2.1}$$

A density matrix can be used to calculate the probability of finding a specific state, in the same way as with the wave function:

$$P(v_\alpha \rightarrow v_\beta) \quad = \quad \left| \langle\psi_\beta|\psi_\alpha\rangle \right|^2 \quad = \quad \langle\psi_\beta|\psi_\alpha\rangle \langle\psi_\alpha|\psi_\beta\rangle \quad = \quad \langle\psi_\beta| \rho |\psi_\beta\rangle \,. \tag{2.2}$$

The probability of finding a specific flavor is thus given by the diagonal elements of the density matrix expressed in the flavor basis. In eq. 2.2 $\langle\psi_\beta| \rho |\psi_\beta\rangle$ simply accesses the diagonal element that corresponds to flavor β. It is required that $Tr(\rho) = 1$ to preserve unitary probabilities, as the sum of finding some neutrino flavor should always be one, otherwise neutrinos will have some chance of oscillating into something that is not one of the considered flavors.

The density matrix for a mixed state can be expressed as a weighted sum over pure state density matrices [8, 9]

$$\rho_{mix} \quad = \quad \sum_n p_n |\psi_n\rangle \langle\psi_n| \,, \tag{2.3}$$

where p_n gives the probability of finding a specific state, and n denotes the individual pure states that contributes to ρ_{mix}.

So far the density matrix has been expressed in the flavor basis of the system. It can also be expressed in the mass basis. The two bases are related by a rotation matrix U, of which the details are described in section 2.4. The rotation of a density matrix from one basis to another is equivalent to rotating the wave functions it consists of (which is given by eq. 2.26)

$$\rho_m = U\left|\psi_\alpha\right\rangle\left\langle\psi_\alpha\right|U^\dagger = U\rho_f U^\dagger, \tag{2.4}$$

where the subscripts m and f denote the mass and flavor bases respectively.

2.1.1 Time evolution of density matrices

To describe the propagation of a particle one has to know how the system evolves in time. The time evolution of a wave function [8] is given by the Schrödinger equation:

$$i\hbar\frac{\partial}{\partial t}\left|\psi\right\rangle = H\left|\psi\right\rangle \quad , \quad -i\hbar\frac{\partial}{\partial t}\left\langle\psi\right| = \left\langle\psi\right|H. \tag{2.5}$$

This can also be applied to a density matrix using the product rule:

$$\begin{aligned} i\hbar\frac{\partial}{\partial t}\rho &= i\hbar\left(\frac{\partial}{\partial t}\left|\psi\right\rangle\left\langle\psi\right| + \left|\psi\right\rangle\frac{\partial}{\partial t}\left\langle\psi\right|\right) = i\hbar\left(\frac{H}{i\hbar}\left|\psi\right\rangle\left\langle\psi\right| + \left|\psi\right\rangle\left\langle\psi\right|\frac{-H}{i\hbar}\right) \\ &= H\rho - \rho H = [H,\rho]. \end{aligned} \tag{2.6}$$

An expression for the time dependent density matrix $\rho(t)$ is then found by integrating both sides of the equation from 0 to t:

$$\begin{aligned} i\hbar\int_0^t \frac{\partial}{\partial t}\rho(t)\mathrm{d}t &= \int_0^t H\rho(t) - \rho(t)H\mathrm{d}t \quad \Rightarrow \\ i\hbar[\rho(t) - \rho(0)] &= \int_0^t H\rho(t) - \rho(t)H\mathrm{d}t \quad \Rightarrow \\ \rho(t) &= \rho(0) - \frac{i}{\hbar}\int_0^t H\rho(t) - \rho(t)H\mathrm{d}t. \end{aligned} \tag{2.7}$$

Solving this differential equation gives $\rho(t)$. The solution for neutrino oscillations in vacuum is given by applying the time shift operator [10] $Q(t)$:

$$Q(t) = e^{\frac{-i}{\hbar}Ht}. \tag{2.8}$$

Then the time evolution of the density matrix becomes:

$$\rho(t) = Q(t)\rho(0)Q(t)^\dagger. \tag{2.9}$$

For more advanced models it might be impractical to find an analytic solution. Time evolution of the density matrix would then be found by numerically solving the matrix differential equation that gives $\rho(t)$.

2.2 The neutrino Hamiltonian

To get the time evolution of a quantum system given by the shrödinger equation (eq 2.5) one needs to know the Hamiltonian, which accounts for the total energy. The time evolution is added to the wave function in the mass basis as particles propagate as mass eigenstates. For a specific state this is given by

$$|\psi(t)\rangle = e^{-iHt}|\psi(0)\rangle = e^{-iEt}|\psi(0)\rangle , \tag{2.10}$$

where E is the energy of the particle given by the formula $E = \sqrt{m^2c^4 + p^2c^2}$ and t is time. In natural units $c = 1$ and the energy becomes:

$$E = \sqrt{m^2 + p^2}. \tag{2.11}$$

This can be expanded using the binomial expansion:

$$(x+y)^n = \sum_k \begin{bmatrix} n \\ k \end{bmatrix} x^{n-k}y^k \quad , \quad \begin{bmatrix} n \\ k \end{bmatrix} = \frac{n!}{k!(n-k)!}. \tag{2.12}$$

An approximation can be made by only using the first few terms in the expansion:

$$E = (p^2+m^2)^{1/2} = p + \frac{m^2}{2p} - \frac{m^4}{4p^3} + \ldots \simeq p + \frac{m^2}{2p}. \tag{2.13}$$

Since $m \ll p$ the $m^2/2p$ term in the expansion is small and $m^4/4p^3$ is negligible. The remaining terms will be even smaller than the third since p appears in an increasingly negative power.

In the final Hamiltonian the term that only includes p is often left out, since this cancels out anyways when calculating the probability of finding a specific flavor. How this happens can be seen in the example in section 2.3:

$$E = \frac{m^2}{2p}. \tag{2.14}$$

The ultra-relativistic approximation $p \simeq E$ can be made due to the low mass of the neutrinos. The Hamiltonian can be expressed in matrix form with the shape NxN, where N is the number of neutrinos:

$$H = \sum_{i=1}^{n} E|\nu_i\rangle\langle\nu_i| = \sum_{i=1}^{n} \frac{m_i^2}{2E}|\nu_i\rangle\langle\nu_i| . \tag{2.15}$$

2.3 A two neutrino example

The following depicts how density matrix formalism and the Hamiltonian found in eq. 2.15 can be used to calculate standard neutrino oscillation probabilities. This also illustrates how the mixing between flavor and mass states gives rise to oscillations. In this example the focus will be on calculating the survival probability of an electron neutrino, considering an approximation where only two neutrino flavors ν_e and ν_μ propagate in vacuum. Natural units will be used throughout the section.

The density matrix for an electron neutrino expressed in the flavor basis is given by eq. 2.1:

$$\rho_f = |\nu_e\rangle\langle\nu_e| = \begin{bmatrix}1\\0\end{bmatrix}\cdot\begin{bmatrix}1 & 0\end{bmatrix} = \begin{bmatrix}1 & 0\\0 & 0\end{bmatrix}. \tag{2.16}$$

This can be rotated into the mass basis by using eq. 2.4

$$\begin{aligned}\rho_m = U\rho_f U^\dagger &= \begin{bmatrix}\cos(\theta) & \sin(\theta)\\-\sin(\theta) & \cos(\theta)\end{bmatrix}\begin{bmatrix}1 & 0\\0 & 0\end{bmatrix}\begin{bmatrix}\cos(\theta) & -\sin(\theta)\\\sin(\theta) & \cos(\theta)\end{bmatrix}\\ &= \begin{bmatrix}\cos^2(\theta) & -\cos(\theta)\sin(\theta)\\-\cos(\theta)\sin(\theta) & \sin^2(\theta)\end{bmatrix},\end{aligned} \tag{2.17}$$

where U is the two-flavor mixing matrix that is characterized by the angle θ. It is the standard matrix describing a rotation of coordinates in two dimensions. Using the convention $\cos(\theta) = c, \sin(\theta) = s$ for simplicity:

$$\rho_m = \begin{bmatrix}c^2 & -cs\\-cs & s^2\end{bmatrix}. \tag{2.18}$$

The time evolution of the density matrix in the mass basis is expressed by using eq. 2.9

$$\rho_m(t) = Q(t)\rho_m Q(t)^\dagger = e^{-iHt}\begin{bmatrix}c^2 & -cs\\-cs & s^2\end{bmatrix}e^{iHt}, \tag{2.19}$$

where H is the Hamiltonian projected on to the mass basis given by eq. 2.15. The p from eq. 2.13 is included here to display how it cancels out, and the ultra relativistic approximation $p \simeq E$ is used:

$$\begin{aligned}H = \sum_{i=1}^{2} E + \frac{m_i^2}{2E}|\nu_i\rangle\langle\nu_i| &= \left(E + \frac{m_1^2}{2E}\right)\begin{bmatrix}1\\0\end{bmatrix}\begin{bmatrix}1 & 0\end{bmatrix} + \left(E + \frac{m_2^2}{2E}\right)\begin{bmatrix}0\\1\end{bmatrix}\begin{bmatrix}0 & 1\end{bmatrix}\\ &= \begin{bmatrix}E + \frac{m_1^2}{2E} & 0\\0 & E + \frac{m_2^2}{2E}\end{bmatrix}.\end{aligned} \tag{2.20}$$

$\rho_m(t)$ then takes the form

$$\begin{aligned}\rho_m(t) &= \begin{bmatrix} e^{-i(E+\frac{m_1^2}{2E})t} & 0 \\ 0 & e^{-i(E+\frac{m_2^2}{2E})t} \end{bmatrix} \begin{bmatrix} c^2 & -cs \\ -cs & s^2 \end{bmatrix} \begin{bmatrix} e^{i(E+\frac{m_1^2}{2E})t} & 0 \\ 0 & e^{i(E+\frac{m_2^2}{2E})t} \end{bmatrix} \\ &= \begin{bmatrix} c^2 & -cse^{\frac{-i(m_1^2-m_2^2)t}{2E}+\frac{-i(E-E)t}{2E}} \\ -cse^{\frac{i(m_1^2-m_2^2)t}{2E}+\frac{i(E-E)t}{2E}} & s^2 \end{bmatrix} \\ &= \begin{bmatrix} c^2 & -cse^{\frac{-i(m_1^2-m_2^2)t}{2E}} \\ -cse^{\frac{i(m_1^2-m_2^2)t}{2E}} & s^2 \end{bmatrix}. \end{aligned} \tag{2.21}$$

A transformation back to the flavor basis is needed, to get the probability of finding a specific flavor at a time t:

$$\begin{aligned}\rho_f(t) &= U^\dagger \rho_m(t) U \\ &= \begin{bmatrix} c & -s \\ s & c \end{bmatrix} \begin{bmatrix} c^2 & -cse^{\frac{-i(m_1^2-m_2^2)t}{2E}} \\ -cse^{\frac{i(m_1^2-m_2^2)t}{2E}} & s^2 \end{bmatrix} \begin{bmatrix} c & s \\ -s & c \end{bmatrix}. \end{aligned} \tag{2.22}$$

Index $(1,1)$ in $\rho_f(t)$, $\rho_f^{11}(t)$, gives the probability of finding the election neutrino at time t (eq. 2.2), or equivalently $1-\rho_f^{22}(t)$ if assuming unitarity of the mixing matrix and conservation of probability, i.e. $(Tr[\rho_f(t)] = 1)$

$$\begin{aligned}P(\nu_e \to \nu_e) &= 1 - \langle \nu_\mu | \, \rho_f(t) \, | \nu_\mu \rangle \\ &= 1 - \begin{bmatrix} 0 & 1 \end{bmatrix} \rho_f(t) \begin{bmatrix} 0 \\ 1 \end{bmatrix} = 1 - \rho_f^{22}(t). \end{aligned} \tag{2.23}$$

I will focus on the term $\rho_f^{22}(t)$ because the entire expression for $\rho_f(t)$ is lengthy and complicated:

$$\begin{aligned}\rho_f^{22}(t) &= s^2c^2\left(e^{\frac{im_1^2t}{2E}} - e^{\frac{im_2^2t}{2E}}\right)\left(e^{\frac{-im_1^2t}{2E}} - e^{\frac{-im_2^2t}{2E}}\right) \\ &= s^2c^2\left(2 - 2\cos\left(\frac{t(m_1^2-m_2^2)}{2E}\right)\right) = \sin^2(2\theta)\sin^2\left(\frac{t(m_1^2-m_2^2)}{4E}\right). \end{aligned} \tag{2.24}$$

This is the standard solution for $P(\nu_e \to \nu_\mu)$ when using this two-flavor approximation, which can also be found by approaching the problem with a standard wave function treatment. $P(\nu_e \to \nu_e)$ is then:

$$P(\nu_e \to \nu_e) = 1 - \sin^2(2\theta)\sin^2\left(\frac{t(m_1^2-m_2^2)}{4E}\right). \tag{2.25}$$

Equation 2.25 consists of two $\sin^2$ terms. The first term depends on the mixing angle and has no time dependence. This is just a constant, that determines the amplitude of the oscillation probability function. The second $\sin^2$ term is time-dependent. The difference in neutrino masses squared $(m_1^2 - m_2^2)$ along with the energy of the particle E controls the frequency of oscillation. If there was no difference in mass, this term would just be equal to 1 and there would be no oscillation.

2.4 Mixing matrix and mass splittings

Neutrino mixing was proposed in 1957 by Bruno Pontecorvo [11], who suggested after the discovery of K^0 mixing, that neutrinos could behave in a similar fashion. The theory describing this phenomenon was formulated a few years later in 1962 [12].

In the Standard Model there are three neutrino flavors, named after the corresponding charged leptons that participate in their interactions. The three neutrino flavor states have been experimentally observed to not match the mass states in which the neutrinos propagate. The relation between flavor and mass states is described by a mixing matrix U. It represents the coordinate rotation one has to make, to go from one basis to another. When considering the three known flavors ν_e, ν_μ, and ν_τ, and the corresponding mass states ν_1, ν_2 and ν_3 the rotation is given by

$$\begin{bmatrix}\nu_e\\ \nu_\mu\\ \nu_\tau\end{bmatrix} = U\begin{bmatrix}\nu_1\\ \nu_2\\ \nu_3\end{bmatrix}, \quad \begin{bmatrix}\nu_1\\ \nu_2\\ \nu_3\end{bmatrix} = U^\dagger\begin{bmatrix}\nu_e\\ \nu_\mu\\ \nu_\tau\end{bmatrix}. \tag{2.26}$$

In a three neutrino framework this matrix is called the PMNS (Pontecorvo-Maki-Nakagawa-Sakata) matrix. This is a unitary matrix, assuming there is no mixing into other presently undiscovered neutrinos:

$$\begin{aligned} U_{PMNS} &= \begin{bmatrix}U_{e1} & U_{e2} & U_{e3}\\ U_{\mu1} & U_{\mu2} & U_{\mu3}\\ U_{\tau1} & U_{\tau2} & U_{\tau3}\end{bmatrix} \\ &= \begin{bmatrix} c_{12}c_{13} & s_{12}c_{13} & s_{13}e^{-i\delta}\\ -s_{12}c_{23} - c_{12}s_{13}s_{23}e^{i\delta} & c_{12}c_{23} - s_{12}s_{13}s_{23}e^{i\delta} & c_{13}s_{23}\\ s_{12}s_{23} - c_{12}s_{13}c_{23}e^{i\delta} & -c_{12}s_{23} - s_{12}s_{13}c_{23}e^{i\delta} & c_{13}c_{23}\end{bmatrix}. \end{aligned} \tag{2.27}$$

The convention $\cos(\theta_{ij}) = c_{ij}$ and $\sin(\theta_{ij}) = s_{ij}$ has been used here. The PMNS matrix has four free parameters: the three mixing angles, θ_{12}, θ_{13}, θ_{23}, and the Charge-Parity (CP) violating phase δ. This can be separated into three different matrices, one for each mixing angle:

$$U_{PMNS} = \begin{bmatrix}1 & 0 & 0\\ 0 & c_{23} & s_{23}\\ 0 & -s_{23} & c_{23}\end{bmatrix}\begin{bmatrix}c_{13} & 0 & s_{13}e^{-i\delta_{cp}}\\ 0 & 1 & 0\\ -s_{13}e^{i\delta_{cp}} & 0 & c_{13}\end{bmatrix}\begin{bmatrix}c_{12} & s_{12} & 0\\ -s_{12} & c_{12} & 0\\ 0 & 0 & 1\end{bmatrix}. \tag{2.28}$$

The mixing angles define how much a neutrino mixes with the other flavors. There are two special values for mixing angles, namely $0°$ and $45°$. When considering an approximate model with only two neutrinos (two-flavor approximation), an angle of $0°$ means no mixing between the two flavors, i.e a neutrino initially created as an electron neutrino will not oscillate into a muon neutrino. When the mixing angle is $45°$, the flavors are maximally mixed and in this case the initially created flavor will oscillate back and forth between entirely being one of the two flavors.

The three-flavor case is more complex, as the oscillation probability depends on multiple angles. If $\theta_{12} = 0$, $\theta_{13} \neq 0$ and $\theta_{23} \neq 0$ for example, the probability of a neutrino initially created as ν_e oscillating into ν_μ is non-zero because ν_e mixes with ν_τ which mixes with ν_μ. In essence the mixing angles determine the amplitude of the wave function describing the probability of finding a given flavor. The angles are sometimes labeled differently, depending on the type of experiment that is sensitive to a specific angle. Solar neutrino experiments are mainly sensitive to θ_{12} and for this reason θ_{12} is also called θ_{sol}. Similarly, atmospheric neutrino experiments are mainly sensitive to $\theta_{23} = \theta_{atm}$.

Neutrino oscillations in vacuum are fully described in terms of the three mixing angles, the mass splittings $\Delta m^2_{ij} = m^2_i - m^2_j$, the CP-violating phase δ_{cp} and the energy of the neutrino. As with the mixing angles, mass splittings can also be labeled according to the type of experiments that are sensitive to a given parameter. The current best fit values for the parameters are listed in table 2.1. There are two best fit values for each

Parameter	Best fit $\pm 1\sigma$ (NO)	Best fit $\pm 1\sigma$ (IO)
θ_{12}	$33.62^{+0.78}_{-0.76}$	$33.62^{+0.78}_{-0.76}$
θ_{13}	$8.54^{+0.15}_{-0.15}$	$8.58^{+0.14}_{-0.14}$
θ_{23}	$47.2^{+1.9}_{-3.9}$	$48.1^{+1.4}_{-1.9}$
$\frac{\Delta m^2_{21}}{10^{-5}eV^2}$	$7.40^{+0.21}_{-0.20}$	$7.40^{+0.21}_{-0.20}$
$\frac{\Delta m^2_{3i}}{10^{-3}eV^2}$	$2.494^{+0.033}_{-0.031}$	$-2.465^{+0.032}_{-0.031}$
δ_{cp}	234^{+43}_{-31}	278^{+26}_{-29}

Table 2.1. – Best fit values for oscillation parameters and their 1σ uncertainty, in the case of a normal (NO) and inverted (IO) mass ordering. Note that Δm^2_{31} and Δm^2_{32} has the same best fit values, both given as Δm^2_{3i}. Table values taken from Ref. [13]

oscillation parameter due to the undetermined mass ordering of neutrinos. It is unknown whether the mass ordering is normal, where $m_1 < m_2 < m_3$ as with quarks and charged leptons, or inverted, where $m_3 < m_1 < m_2$. This remains one of the big questions left in neutrino physics.

Oscillations occur because the neutrinos have non-zero masses. This gives rise to an oscillatory term in the probability of finding a neutrino flavor at a given time after it has been created, as seen in the example in section 2.3. In the two-flavor approximation the probability of finding the initially created neutrino after a time t is given by eq. 2.25

$$P(\nu_e \to \nu_e) \quad = \quad 1 - \sin^2(2\theta)\sin^2\left(\frac{t(m_1^2 - m_2^2)}{4E}\right). \tag{2.29}$$

The second $\sin^2$ term depends on the difference in squared masses, and along with the energy this defines the frequency of oscillation. The sign of $m_1^2 - m_2^2$ cannot be determined from this equation alone since $\sin^2$ is an even function. As a consequence the two mass orderings give the same oscillation probability. The value of Δm_{21}^2 has been determined to be positive by solar neutrino experiments [14] implying that $m_1 < m_2$, and thus only the sign of Δm_{32}^2 and Δm_{31}^2 is unknown.

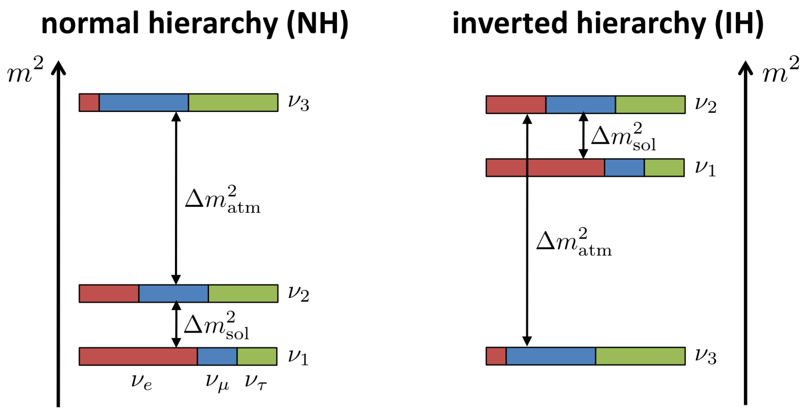

Figure 2.1. – Illustration of the possible orderings of the neutrino masses. (Taken from Ref. [15])

As seen in table 2.1, Δm_{21}^2 has a value comparable to 2σ of Δm_{3i}^2. A more precise measurement of Δm_{3i}^2 is needed to determine the mass ordering.

3 IceCube neutrino observatory

The IceCube neutrino observatory is the largest neutrino detector in the world. It consists of one cubic kilometer of instrumented ice located at the geographic South Pole. A sketch of the detector is shown in figure 3.1. The ice contains vertical 86 strings situated approximately 125 meters apart in a hexagonal grid, each with 60 Digital Optical Modules (DOMs) attached. The DOMs are located between 1450 and 2450 meters below the surface, where the ice is very clear and devoid of sunlight.

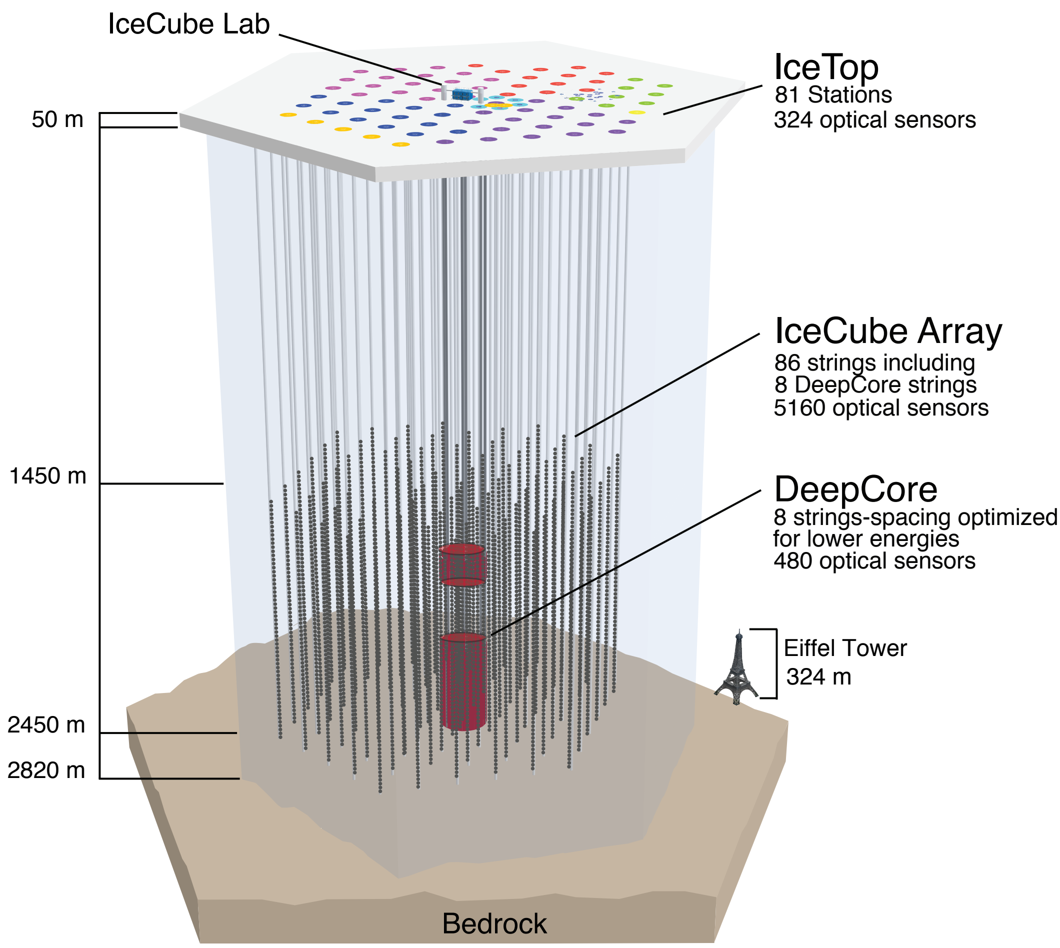

Figure 3.1. – Sketch of IceCube neutrino observatory with DeepCore. The top of each string is color coded according to which season they were deployed [16].

The ice is more densely instrumented in the central region of IceCube, known as DeepCore [17] (highlighted in red on figure 3.1). This enables DeepCore to probe lower energies than rest of the detector. DeepCore is sensitive to neutrinos with energies down to around $5 GeV$, and is more efficient at detecting neutrinos below $150 GeV$ than IceCube.

3.1 Digital optical modules

The detection units in IceCube are known as DOMs [18]. They consist of a 10-inch Photo Multiplier Tube (PMT) situated inside a glass sphere along with the electronics main board, and a flasher board with diodes located around the edge. An overview of the DOM can be seen in figure 3.2. The PMTs have a quantum efficiency of around 25 percent, which makes them sensitive to single photons. The ones situated on DeepCore strings have a higher quantum efficiency of approximately 35 percent, which increases the sensitivity of DeepCore further. The signal from a photon hitting the PMT is amplified by a factor of 10^7 to convert a single electron into a measurable current.

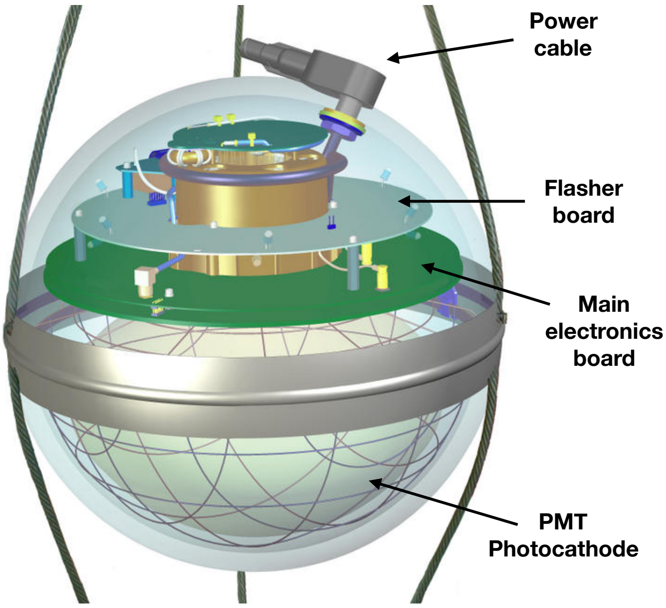

Figure 3.2. – Digital optical module and the most important components.

The DOM is launched, meaning that its starts "recording", when a signal corresponding to more than 0.25 photoelectrons is received. This starts digitization of the signal in two different waveform digitizers, the Analog Transient Waveform Digitizer (ATWD) and the fast Analog-to-Digital Converter (fADC). The ATWD is recording with a binning of approximately $3.3ns$, with a total of 128 bins. This recording is only kept if the nearest or next-to-nearest DOM is launched within $1\mu s$ of the original hit. Such a coincidence is know as a Hard Local Coincidence (HLC) pair. It is more likely that an event launching multiple DOMs is not caused by noise. The fine binning is required to more accurately reconstruct the number of photons received in such events. Each DOM has two ATWDs in case another HLC event occurs within the readout time of the ATWD digitizing the initial event.

The fADC provides a continuous readout with a lower resolution to capture the basics of Soft Local Coincidence (SLC) hits. Only a time stamp and minimal information about the charge is kept for these events.

Each DOM also contains a flasher board with 12 light-emitting diodes that can be remotely activated. They are used to send out light pulses for studying the optical ice properties. By using flashers, an estimation for scattering and absorption length can be made as a function of depth in the ice, which is important for reconstructing neutrino events more precisely. Furthermore, other effects like cables blocking the light from certain directions, or DOMs being slightly tilted can be investigated.

3.2 Neutrino sources

The neutrinos detected by IceCube/DeepCore come primarily from two sources; cosmic ray interactions in the atmosphere, and astrophysical neutrino sources which are currently unknown, although recent find of correlation between astrophysical neutrinos and a blazar [19] is the first step towards characterizing these sources. The two types are known as atmospheric and astrophysical neutrinos respectively.

Atmospheric neutrinos have the advantage that the point of creation, and thus distance traveled before reaching the detector, is somewhat known. The incoming angle in the detector reveals from where on the Earth they originate, and the distance traveled can be estimated as length of a direct path between that point and IceCube. The known distance to the point where the neutrinos are created is important for this analysis, for reasons that will be clarified in section 4.3.

3.3 Neutrino detection

Neutrinos have an extremely small cross section compared to all other Standard Model particles. Most of them go right through IceCube/DeepCore and the rest of the Earth without interacting. Occasionally a neutrino interacts with one of the nucleons or electrons in the ice. The probability for this happening is highly dependent on the neutrinos energy, which can be seen in figure 3.3. Note that the y-axis displays $\frac{\text{cross section}}{\text{neutrino energy}}$; interaction probability rises with energy.

Neutrinos interact via different processes at different energies. The dominant interaction type at the energies IceCube is sensitive to is Deep Inelastic Scattering (DIS), where the neutrino interacts with a quark inside a nucleon. This interaction always results in a hadronic shower. The two other interaction types, Quasi-Elastic scattering (QE) and Resonant Scattering (RES), are heavily suppressed with energy as seen in figure 3.3.

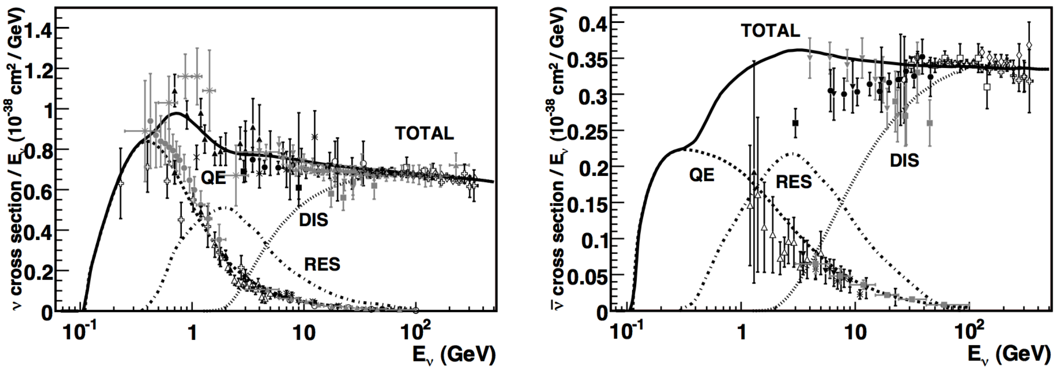

(a) **(b)**

Figure 3.3. – Different components contributing to the neutrino (left) and anti-neutrino (right) cross section. The total cross section is dominated by DIS above $10GeV$. Taken from [20].

Neutrinos only interact via the weak nuclear force, which limits the interactions to two types: the charged current (CC) interaction where a W^+ or W^- boson is exchanged, and the neutral current (NC) with the exchange of a Z boson. Feynman diagrams of the two interaction types can be seen in figure 3.4

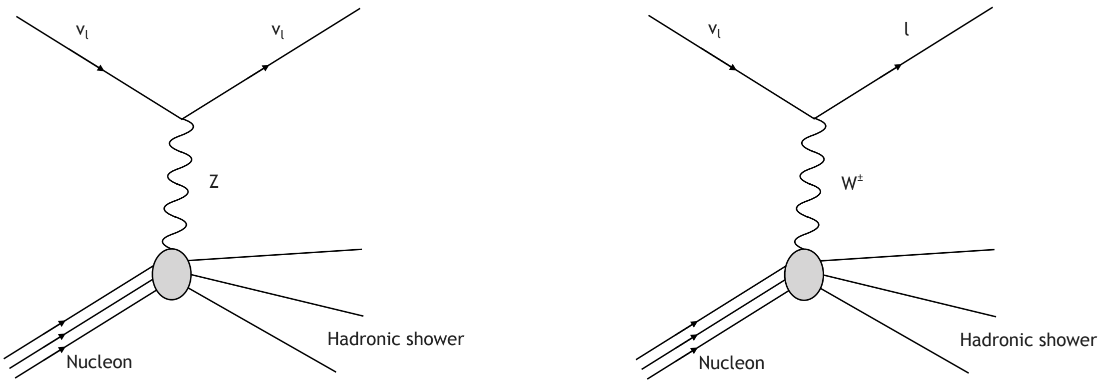

Figure 3.4. – Feynman diagrams of a neutral current (left) and charged current (right) neutrino DIS interaction.

The neutrino interacts primarily with the quarks inside protons and neutrons at the energies IceCube/DeepCore is sensitive to, in both NC and CC interactions. The energy transfer is large enough to break the nucleon apart, forcing the creation of additional particles due to color confinement, which results in a hadronic shower. A lepton with its flavor corresponding to the neutrino interacting is created in CC interactions. The lepton travels faster than the speed of light in ice at the energies IceCube is sensitive to. This releases a super-luminal boom, also know as Cherenkov radiation.

IceCube events are divided into two types called tracks and cascades. The difference between the two event types can be seen in figure 3.5. In practice, all interactions except the ν_μ CC interaction have the light signature known as a cascade.

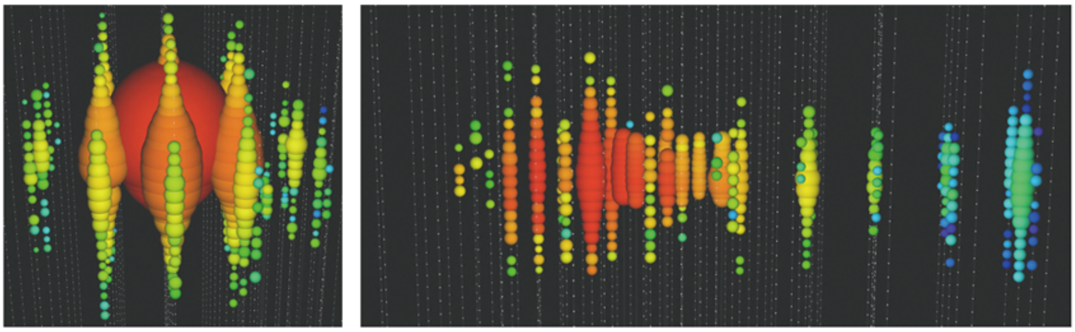

Figure 3.5. – A cascade event (left) and a track event (right) displayed in the IceCube event display. Each DOM is marked by a small white dot. The size of each colored ball indicates how much light a DOM has received. The color displays when that DOM was hit by photons, red being earlier and green/blue later.

When an electron is created in a ν_e CC interaction it deposes most of its energy via bremsstrahlung, emitting photons in all direction. Some of these are energetic enough to produce additional electron-positron pairs, which undergo the same process. Taus from ν_τ CC interactions decay before traveling far enough to look like a track. This releases two inseparable cascades very close to each other, one from the neutrino interaction and one from the tau decay. In principle very energetic tau neutrino events with $E > PeV$ should have a so-called "double bang" light signature where the cascades are separated due to the prolonged lifetime of the tau.

Only muons created in ν_μ CC interactions live long, and interact infrequently enough to make the track-like light signature. It should be noted that the taus created in ν_τ CC interactions decay into muons 17% of the time, which can make them look like muon neutrinos.

Neutrinos are never observed directly in IceCube: only the charged particles resulting from neutrino interactions in the ice.

3.3.1 Event reconstruction

The translation from number of photons received by each DOM to the particle quantities vertex position, energy, direction in azimuth and zenith angle, track length, and time, is known as event reconstruction. It happens in a minimization process, where the parameters that gives the highest probability for photons hitting the launched DOMs are chosen.

The separation into the two event types, tracks and cascades, happens with a cut on reconstructed track length at $50m$, everything below being cascades. The ability to distinguish between the two scales with energy, as the recognition of something as a track or cascade is more precisely done when more DOMs are hit by photons during an event.

Event reconstruction is vital for the analysis, due to the separation of neutrinos into different event categories, which makes the distinction between different neutrino flavors clearer.

3.4 Detector backgrounds

The detection of neutrinos is complicated by the presence of other light sources launching the DOMs. These must be characterized in order to separate them from the signal caused by neutrinos. Among the most important unwanted sources are muons created when cosmic rays interact with the atmosphere, and intrinsic noise in the DOMs. The two have distinctive signatures in the detector, which can be used to discriminate them from neutrinos.

3.4.1 Detector noise

Noise originating from within the DOMs have three primary components [21]; thermal noise, correlated noise, and after-pulsing. Each of the three has a distinct timescale and shape that defines the individual characteristics, visualized in figure 3.6. The plot is made using Hitspool data, which consists of local hard drives on the South Pole storing every hit in a buffer for 16 hours [21]. This data storage was implemented for supernova alerts, but is also useful for studying the detector noise, while normal data is triggered and thus already "cleaned" from some of the noise hits.

Thermal noise, also known as uncorrelated noise, is poisson distributed and temperature dependent. It is caused by the random motion of electrons in the electronics. The rate is estimated for each individual DOM, as the temperature varies depending on depth.

Correlated noise is of unknown origin, and has the counter-intuitive property that its frequency increases with decreasing temperature. A burst of photons is released within a short time span, hence the name "correlated". It has been hypothesized that the origin might be radioactive decays in the glass of the DOM and PMT.

After-pulsing is caused by electrons bouncing backwards on one of the dynodes inside a PMT before continuing forwards. This creates a delay in the arrival time between the original electron bunch, and the electrons coming with the one that has bounced backwards once. As a consequence a small signal will be received with a delay with respect to the initial electrons arrival.

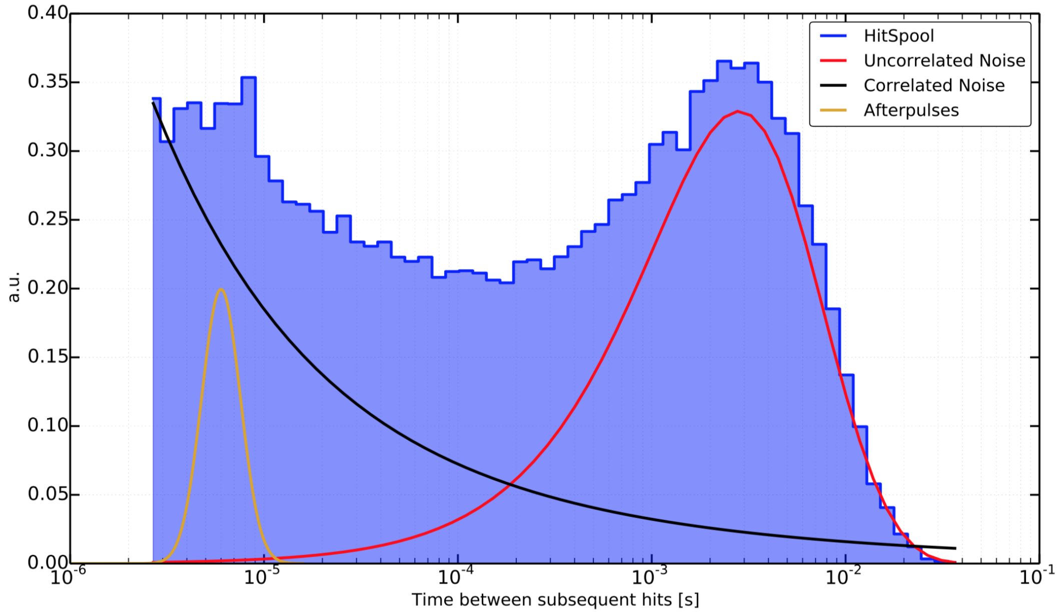

Figure 3.6. – The different components of noise plotted on top of HitSpool data from a single DOM. Taken from [22].

3.4.2 Cosmic ray muons

The Earth's atmosphere is constantly bombarded from space by cosmic rays. Cosmic rays consist of a variety of particles ranging from single electrons to heavy nuclei, but are mainly protons and alpha particles. These have kept their original (but misleading) name "rays", from an era where they were thought to be electromagnetic radiation. Muons are one of the products created in interactions between cosmic rays and the Earth's atmosphere. The ones that reach the detector will create a track like light signature, just like muons coming from ν_μ CC interactions.

Cosmic-ray muons can be identified in a number of ways. A muon cannot penetrate very far through the Earth due to its short lifetime and large cross section (compared to neutrinos). For this reason, their track signatures will always be down-going or close to horizontal. If a muon is created from a neutrino interaction in the ice above the detector it cannot be distinguished from a comic-ray muon, since the same particle is seen in both cases. However if the track starts inside the detector or is up-going, the muon must come from a neutrino interaction. In this case the muon cannot have been created in the atmosphere above, as the track would be down-going and connected to the edge of the detector.

The flux of cosmic rays (and thus muons) depends on energy. The cosmic ray spectrum for high energy cosmic rays can be seen in figure 3.7.

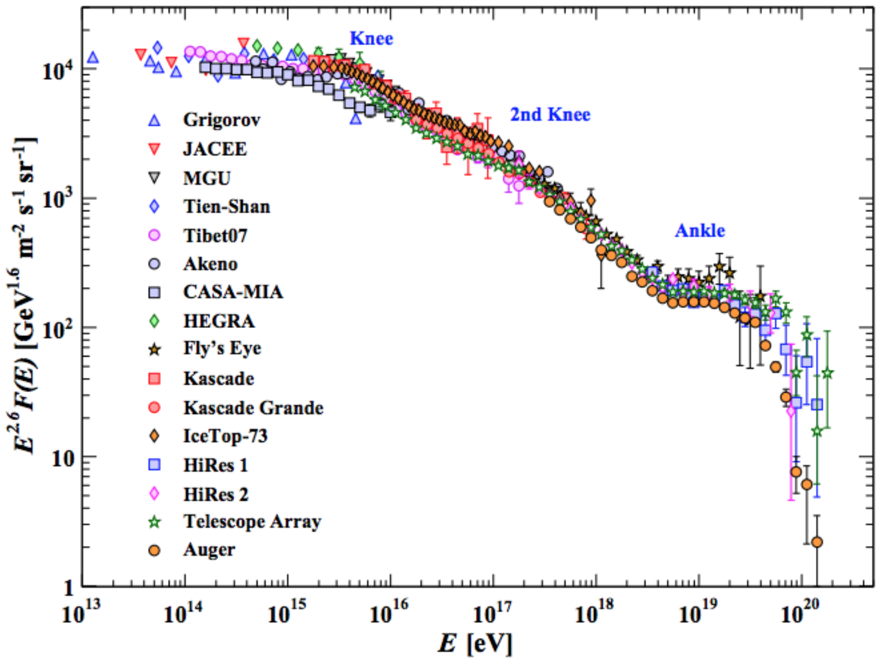

Figure 3.7. – The flux of cosmic rays as function of energy per nucleus. Taken from [23].

The flux of cosmic ray muons and atmospheric neutrinos should have approximately the same energy dependence, since they both come from the same source, namely pions created in cosmic ray interactions. There should be roughly two muon neutrinos and one electron neutrino for each cosmic ray muon, as all three particles come primarily from pion decays.

4 Decoherence

Quantum systems are often idealized and treated as isolated from its surroundings when calculating their properties, but this is rarely true in nature. In reality, they exist and propagate in a sea of other particles, such as photons, electrons, nuclei, or microscopic black holes. This gives a non-zero probability of undergoing some interaction with the surrounding environment, either via one of the force carriers, or by some other mechanism [24]. The knowledge about how the initial system was prepared is partially or fully lost by this interaction, as the system is modified or "measured" at this point. This causes a loss of information about its state, also known as decoherence.

The idea that neutrinos may decohere has been around for almost as long as neutrino oscillations, and has been considered an alternative hypothesis for explaining the previously unknown cause of missing neutrinos in the solar neutrino problem described in section 1.1. It has since been established that neutrinos do in fact oscillate, but this does not rule out that decoherence could still be present as a sub-leading effect.

Throughout this project a decoherence caused by some coupling to the environment is considered. There are other effects that could cause decoherence, e.g. separation of neutrino wave packets in space due to the difference in masses. While this is also very interesting, it will not be discussed in this work.

The following is meant to give a basic understanding of how decoherence effects could arise, before diving into the derivation of an equation describing the phenomenon.

4.1 Decoherence toy model

Neutrino decoherence can be understood as one or more "interactions" along the way of propagation. The particular origin of this contact with the environment is not assumed in this project, but examples include quantum gravity models in which particles can interact with vacuum fluctuations [25], or longer travel distance caused by propagating close to microscopic black holes. It is however assumed that this interaction is of beyond Standard Model origin, and is thus not governed by the weak force. Since particles are propagating as their mass states, an interaction caused by a beyond Standard Model mechanism is assumed to affect the propagating states, and would be in the system's mass basis.

An interaction leading to decoherence effects could be in the flavor basis, but this has a lack of motivation. Interactions in the flavor basis are already characterized by the weak nuclear force, and the impact these have on neutrino oscillations are largely known. With that said it is still important to state that the interactions happening in the mass basis is an analysis choice.

The mass basis interaction causes a phase shift in the wave function describing the probability of finding the initially created neutrino after a given length of propagation, in a similar way as an interaction in the flavor basis would. When a neutrino interacts via the weak force, a "measurement" is made, and the flavor of the interacting particle is then known. This shifts the phase such that the probability of finding the interacting neutrino flavor is one (since we just "measured" it as that flavor). An interaction in the mass basis could shift the phase differently, and the probability of finding a specific flavor or mass eigenstate after the interaction does not necessarily have to be one or zero.

A two-flavor toy model with a neutrino initially created as ν_e is shown in figure 4.1. The neutrino interacts in the mass basis at a random distance seen in the figure as a vertical jump. The phase relation with standard neutrino oscillations is then lost, since both the point of interaction and size of the perturbation is unknown.

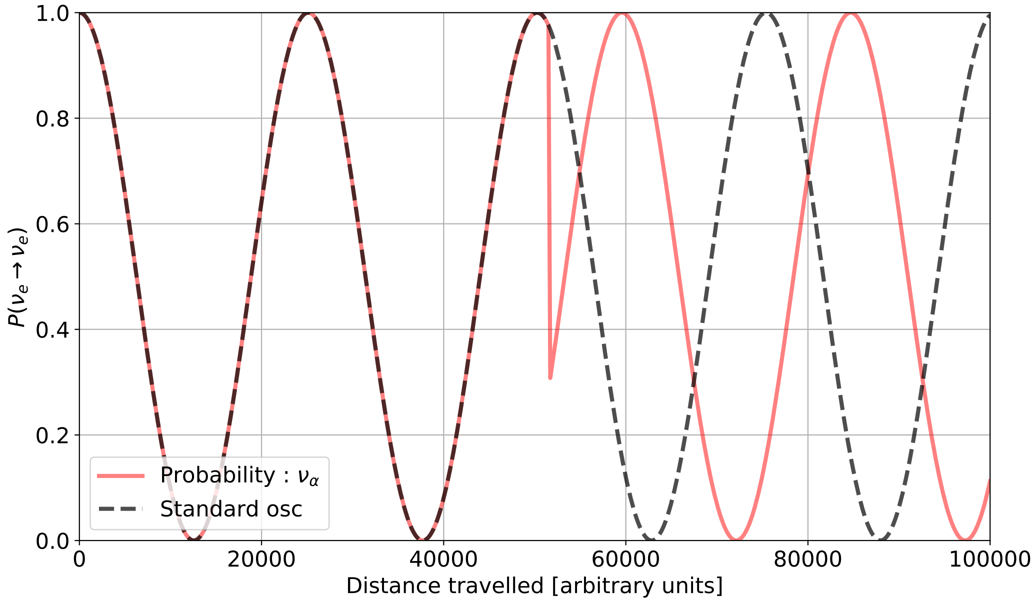

Figure 4.1. – Two-flavor toy model of neutrino decoherence with $\theta = 45°$. The neutrino ν_α loses its phase relation with standard oscillations after the wave function is perturbed by a beyond Standard Model interaction with the environment (vertical jump).

It is easier to see the impact this has on the overall probability of detecting individual flavors when considering more than one neutrino. Figure 4.2 shows an example where three propagating neutrinos are subject to the same mechanisms as before, namely perturbations caused by an interaction in the mass basis. The average probability of finding an electron neutrino is the same as in the standard oscillation picture, until one of the three neutrinos "interacts" and the phase relation with standard oscillations is lost. The combined effect of individual neutrinos interacting at different distances makes the average probability of finding a neutrino as an electron neutrino tend towards 0.5.

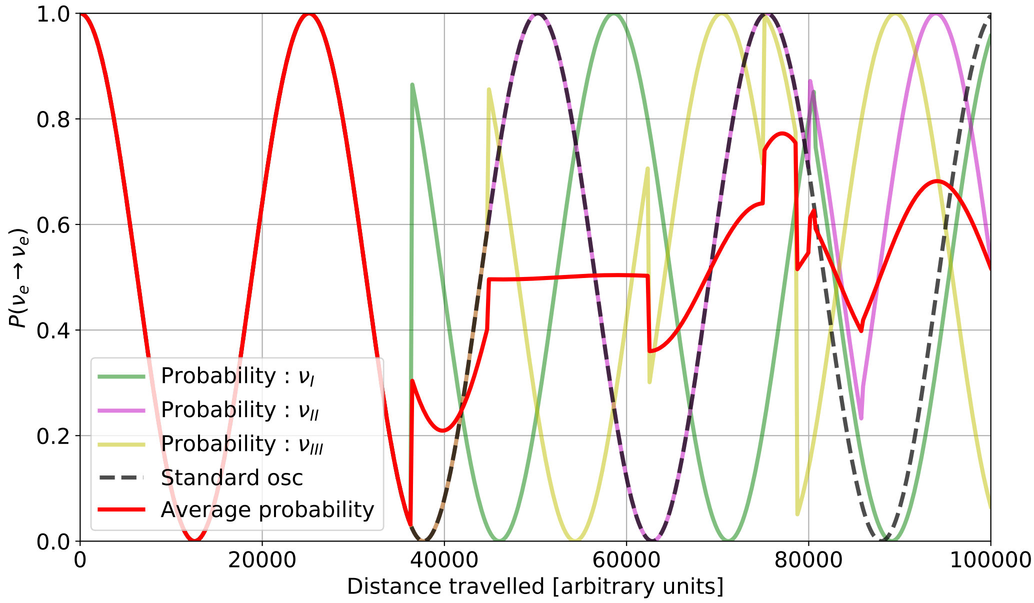

Figure 4.2. – Two-flavor toy model of neutrino decoherence with $\theta = 45°$. This model considers three individual neutrinos ν_I, ν_{II}, and ν_{III} that start as electron neutrinos and interact in the mass basis while propagating. The points of interaction are where the individual neutrino wave functions are discontinuous (vertical jumps).

When considering many neutrinos it becomes clear that decoherence acts as a damping effect on the average oscillation probability. The average probability for finding one of the two flavors goes to the mean of the wave function. The strength of the damping effect results from a combination of mean free path between mass basis interactions, and the size of perturbation that the neutrino wave function undergoes by interacting. This might be a larger change in phase if the interactions collapse the wave function in a similar fashion as when neutrinos interact weakly, or small if the interaction in the mass basis corresponds to one neutrino traveling slightly longer because of a density fluctuation on its path of propagation.

Neutrinos have to interact multiple times to fully decohere if the perturbation is small, because each interaction does not remove all information about the phase relation with standard neutrino oscillations. The phase relation could also be completely lost after a few interactions, if they perturb the wave function by a larger amount. Figure 4.3 displays how many interactions, each of which perturb the wave function by an arbitrarily large amount, make the average probability of detecting an electron neutrino go to 0.5 when considering many neutrinos.

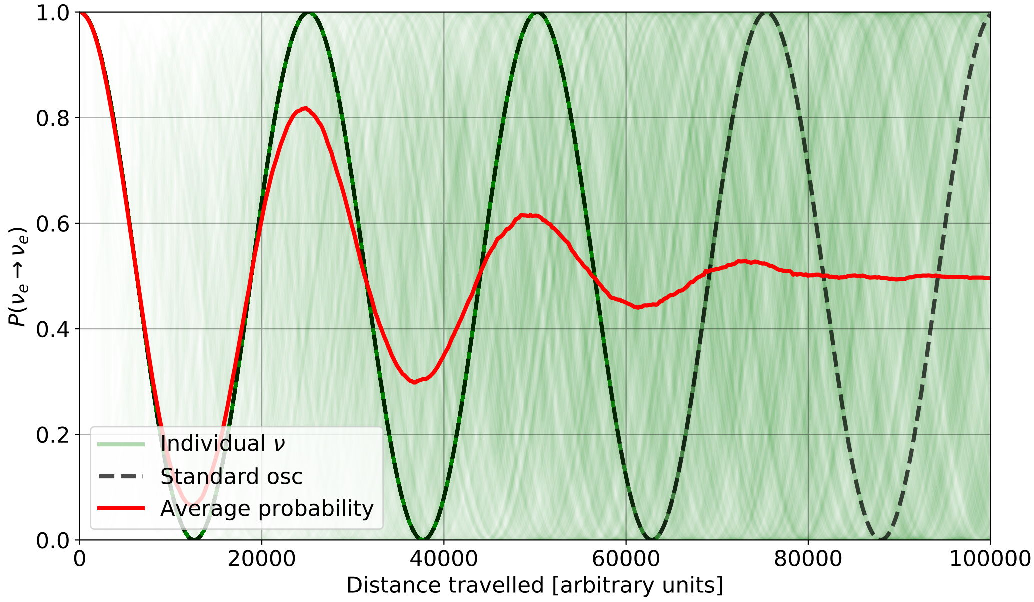

Figure 4.3. – Two-flavor toy model of neutrino decoherence with $\theta = 45°$. The green lines show wave functions for 1000 different neutrinos, which have some probability of being perturbed while propagating.

It should be noted that the average probability of finding a neutrino flavor only tend to 0.5 in the maximally mixed case.

4.2 A phenomenological model of neutrino decoherence

The theoretical treatment of neutrinos in an open quantum system gives rise to an extra term in the equation for a time dependent density matrix (compared to standard neutrino oscillations described by eq. 2.7), known as the decoherence term. The Lindblad equation [26] is considered the most general way of describing the time evolution of an open quantum system using density matrix formalism while preserving trace and complete positivity. It takes into consideration that a quantum system is never fully isolated. The trace of ρ has to be preserved, otherwise a neutrino can oscillate from a specific flavor into something that is not one of the known flavors, meaning that probability vanishes from the system. This could be the case in neutrino decay models, which are not considered here. Complete positivity ensures that the probability given by using this equation is physically interpretable and positive. This is a justifiable assumption as it is hard to interpret negative or imaginary probabilities.

The Lindblad equation describing an N-dimensional system [27], with N being the number of neutrino flavors, can be written as

$$\begin{aligned}\frac{\partial}{\partial t}\rho(t) &= -\frac{i}{\hbar}[H,\rho(t)] + \sum_{n}^{N^2-1} h_n\Big(A_n\rho(t)A_n^\dagger - \frac{1}{2}\{A_nA_n^\dagger,\rho(t)\}\Big) \\ &= -\frac{i}{\hbar}[H,\rho(t)] + D[\rho(t)],\end{aligned} \tag{4.1}$$

where the first term accounts for standard oscillation, and the second term is the decoherence part, with $\{A_nA_n^\dagger,\rho(t)\}$ being the anticommutator of $A_nA_n^\dagger$ and $\rho(t)$. Here, h_n is some positive coefficient and A_n is an N by N matrix that accounts for decoherence effects.

It is assumed that average energy of the system is conserved, which is enforced by making A_n commute with H, and the diagonality of H requires A_n to be diagonal as well. When considering three neutrino flavors A_n takes the form:

$$A_n = \begin{bmatrix} a_{n,1} & 0 & 0 \\ 0 & a_{n,2} & 0 \\ 0 & 0 & a_{n,3}\end{bmatrix}. \tag{4.2}$$

h_n and A_n can be absorbed into the a new variable D_n to simplify the equation. We also have $N^2-1=8$ for three flavors:

$$\begin{aligned} D_n &= \begin{bmatrix} d_{n,1} & 0 & 0 \\ 0 & d_{n,2} & 0 \\ 0 & 0 & d_{n,3}\end{bmatrix} = \frac{\sqrt{h_n}}{\sqrt{2}}A_n \Rightarrow \\ D[\rho(t)] &= -\sum_{n=1}^{8}\Big(\{D_nD_n^\dagger,\rho(t)\} - 2D_n\rho(t)D_n^\dagger\Big).\end{aligned} \tag{4.3}$$

Another assumption is that von Neumann entropy increases which requires D_n to be hermitian ($D_n = D_n^\dagger$). This also implies that $D_nD_n^\dagger = D_n^2$ which can be used to simplify the equation:

$$D[\rho(t)] = -\sum_{n=1}^{8}\Big(D_n^2\rho(t) + \rho(t)D_n^2 - 2D_n\rho(t)D_n\Big). \tag{4.4}$$

The decoherence term in the Lindblad equation now only depends on 8 diagonal D_n matrices and the time dependent density matrix. In matrix form this term becomes:

$$D[\rho(t)] = -\sum_{n=1}^{8}\begin{bmatrix} 0 & (d_{n,1}-d_{n,2})^2\rho_{12}(t) & (d_{n,1}-d_{n,3})^2\rho_{13}(t) \\ (d_{n,2}-d_{n,1})^2\rho_{21}(t) & 0 & (d_{n,2}-d_{n,3})^2\rho_{23}(t) \\ (d_{n,3}-d_{n,1})^2\rho_{31}(t) & (d_{n,3}-d_{n,2})^2\rho_{32}(t) & 0\end{bmatrix}. \tag{4.5}$$

$\sum_{n=1}^{8}(d_{n,i} - d_{n,j})^2$ can be defined as Γ_{ij}. Furthermore $(d_{n,i} - d_{n,j})^2 = (d_{n,j} - d_{n,i})^2$ and this leaves us with three free decoherence parameters Γ_{21}, Γ_{31}, and Γ_{32}, which are damping parameters between each pair of mass states:

$$D[\rho(t)] = -\begin{bmatrix} 0 & \Gamma_{21}\rho_{12}(t) & \Gamma_{31}\rho_{13}(t) \\ \Gamma_{21}\rho_{21}(t) & 0 & \Gamma_{32}\rho_{23}(t) \\ \Gamma_{31}\rho_{31}(t) & \Gamma_{32}\rho_{32}(t) & 0 \end{bmatrix}. \tag{4.6}$$

Expressing $D[\rho(t)]$ in this way has some advantages. The diagonal elements are zero, meaning that total probability of finding a neutrino as one of the three flavors is conserved. This investigation is not sensitive to the individual underlying parameters $d_{n,i}$, which makes it advantageous to have a model with three free decoherence parameters instead of 24 (8 matrices with three diagonal elements in each). The three parameters have some interdependence, as they come from the same underlying parameters. As an example, Γ_{21} and Γ_{31} both depend on the underlying parameters $d_{n,1}$. If one or more of these are changed, both Γ_{21} and Γ_{31} are impacted. This gives a constraint on the values each Γ_{ij} can take. This constraint can be visualized by assigning random values to each of the 24 underlying parameters and then plotting the values that the three Γ parameters take.

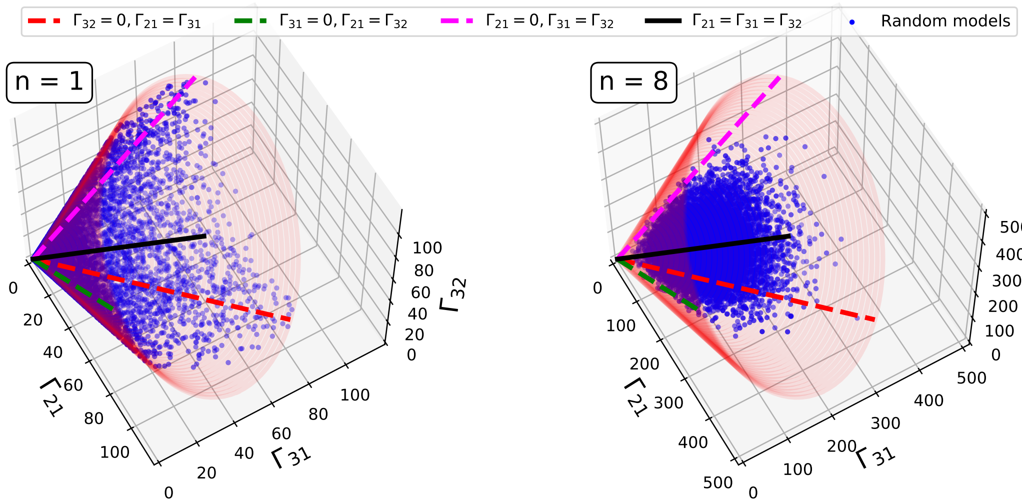

Figure 4.4. – Values that Γ_{21}, Γ_{31}, and Γ_{32} take when the underlying parameters are randomized (blue dots).
Left: Only one of the eight D_n matrices contains non-zero values. All of the points generated are on the surface of the cone defining the Γ parameters bound.
Right: All of the eight D_n matrices contain non-zero values. Every point lies within the conical bound.

As seen on figure 4.4 all valid combinations of the three Γ parameters, meaning Γ_{ij}-values that can be generated when the underlying parameters are real ($d_{n,i} \in \mathbb{R}$), lie within a cone, that is defined by a central line l_c characterized by all points that fulfill

$\Gamma_{21} = \Gamma_{31} = \Gamma_{32}$ (black line on figure 4.4), and an angle between l_c and a line on the surface l_s. l_s can be taken as one of the lines defined by the three special cases where $\Gamma_{21} = \Gamma_{31}, \Gamma_{32} = 0$, $\Gamma_{21} = \Gamma_{32}, \Gamma_{31} = 0$, or $\Gamma_{31} = \Gamma_{32}, \Gamma_{21} = 0$ (colored lines on figure 4.4). It should be noted that the special case where two of the Γ parameters are equal to zero and the third takes a non-zero value is unphysical, because it corresponds to a point outside the conical bound.

4.2.1 Energy-dependent decoherence

The possibility exists for decoherence to be energy dependent, in a similar way as the neutrino weak interaction cross section. The shape of the energy dependence could be anything and thus a simple model is considered here, where a power law characterizes it:

$$\Gamma_{ij} \quad = \quad \Gamma_{0,ij}\left(\frac{E_\nu}{E_0}\right)^n \quad , \quad E_0 = 1GeV \tag{4.7}$$

The exponent n determines the shape of the function. Setting $n = 0$ restores the decoherence model without energy dependence. E_0 is set to $1GeV$, as this is comparable to the neutrino energies considered in this analysis. The scale can be chosen arbitrarily as the purpose is just to characterize the shape of energy dependence.

Another assumption is that the three decoherence parameters have the same energy dependence. This gives the simplest form without introducing more than one extra degree of freedom, and allows energy dependence to be added to the decoherence term as a scalar:

$$\frac{\partial}{\partial t}\rho(t) \quad = \quad -\frac{i}{\hbar}[H, \rho(t)] + D[\rho(t)]\left(\frac{E_\nu}{E_0}\right)^n. \tag{4.8}$$

The value of Γ_{ij} depends on energy when $n \neq 0$. When n is positive the strength of decoherence increases with energy. It is important to differentiate between Γ_{ij} and $\Gamma_{0,ij}$ when considering energy dependent cases. $\Gamma_{0,ij}$ is the absolute value of the decoherence parameter of which a measurement can be made. Γ_{ij} is the energy dependent parameter that varies. It is the effective strength of decoherence at a certain energy.

Figure 4.5 shows the value of Γ_{ij} as a function of neutrino energy for different n. The value of $\Gamma_{0,ij}$ is set to $1feV$, as this value is comparable to but below current limits of neutrino decoherence [28].

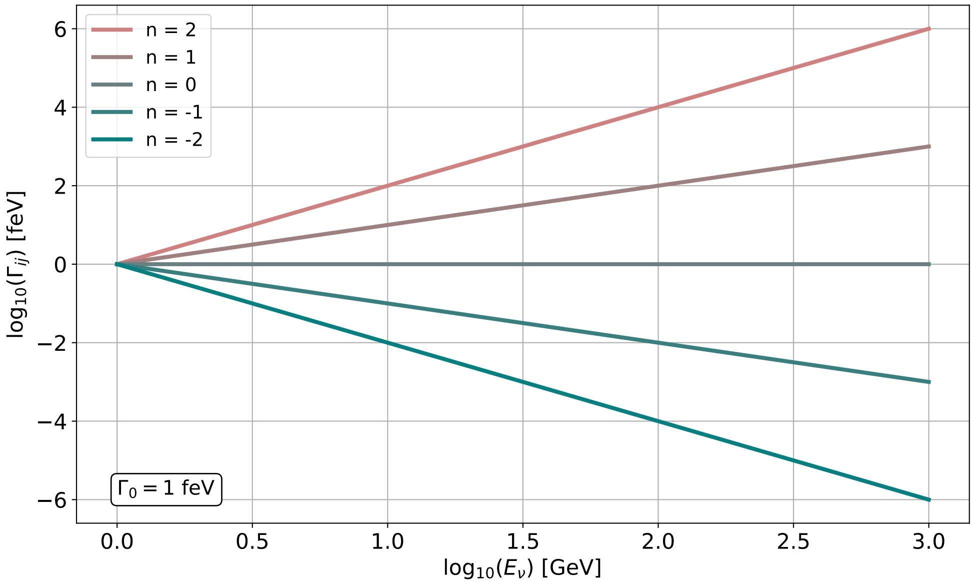

Figure 4.5. – The effective Γ_{ij} value as function of n when using $\Gamma_{0,ij} = 1 feV$.

The decoherence model without energy dependence will be used for illustrative purposes throughout the rest of this chapter, where $\Gamma_{ij} = \Gamma_{0,ij}$. Γ parameters will be listed without the subscript 0 whenever the decoherence model considered is not energy dependent.

4.3 Impacts on neutrino oscillations

The following section will assume a model where $\Gamma_{21} = \Gamma_{31} = \Gamma_{32} = \Gamma$ for visualizing the impact of adding decoherence to neutrino oscillations. It will be discussed later whether or not decoherence is sufficiently described by a single effective parameter.

The effects are shown on oscillations of neutrinos initially created as ν_μ, while this is where decoherence has its biggest impact. Muon neutrinos are also the most distinguishable neutrinos in IceCube. The distance traveled for a muon neutrino can be more accurately reconstructed, due to its track like light signature that gives a good pointing resolution, and the fact that the majority of muon neutrinos are of atmospheric origin. Furthermore $\theta_{23} \simeq 45°$ and has the biggest uncertainty of the three mixing angles, making muon neutrinos a good candidate for probing sub-leading oscillation effects as decoherence. The neutrino energy is generally set to $25 GeV$, while ν_μ has its oscillation maximum around a distance comparable to the Earth's diameter at this energy.

Adding decoherence to the time evolution of neutrinos damps oscillations, as seen in section 4.1. The effect is more complex when considering three neutrinos, instead of two. The probabilities of finding a given flavor at a distance, L, are damped to their average value. How quickly this happens depends on the strength of decoherence parameters. Figure 4.6 shows how this affects a muon neutrino's oscillation probability.

The minimum probability of finding a muon neutrino around $13000km$ is changed in the decoherence model to around 20% instead of 0%.

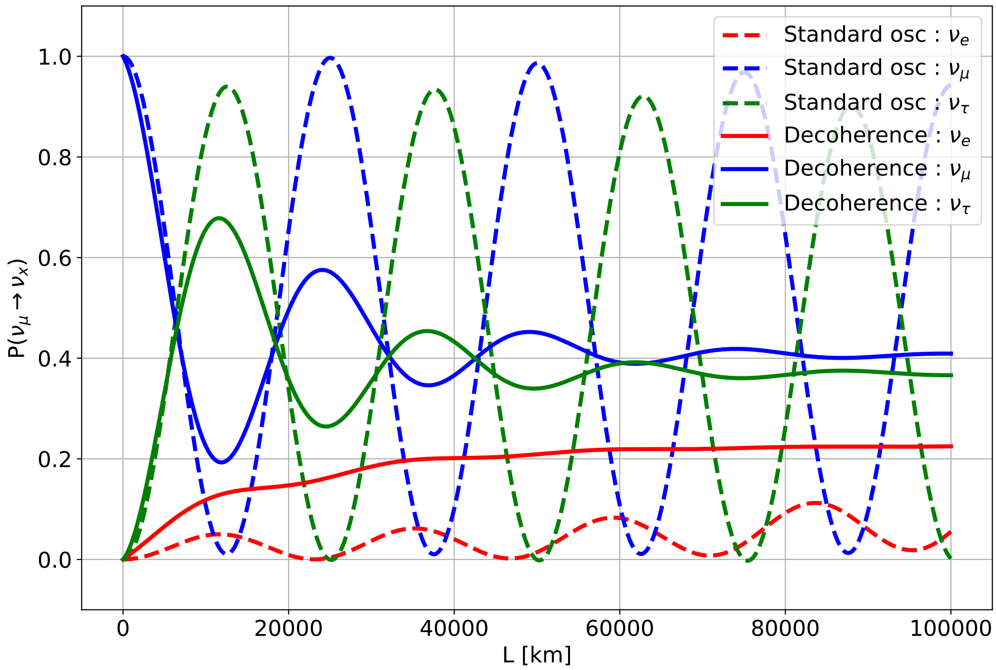

Figure 4.6. – Three-flavor model of neutrino decoherence in vacuum using current best fit values of oscillation parameters from table 2.1 and $E_\nu = 25GeV$. The decoherence parameters have been set to $\Gamma_{21} = \Gamma_{31} = \Gamma_{32} = 10feV$.

The L range shown in figure 4.6 is insufficient to see the fully damped "averaged" oscillation probability. The same models are shown in figure 4.7 to highlight that probabilities tend to the average at large L. The solid blue line displaying $\nu_\mu \rightarrow \nu_\mu$ is damped to the average of the dashed blue, the solid red to the average of the dashed red and so forth. This is an important cross check of the understanding of decoherence effects.

In section 4.1, decoherence is implemented as random perturbations of the oscillation probabilities. The phenomenological model should be able to reproduce the same effect, if the implementation of decoherence is correct. The distances considered here are not relevant for atmospheric neutrinos used in the analysis, but are included for illustration and as a sanity check.

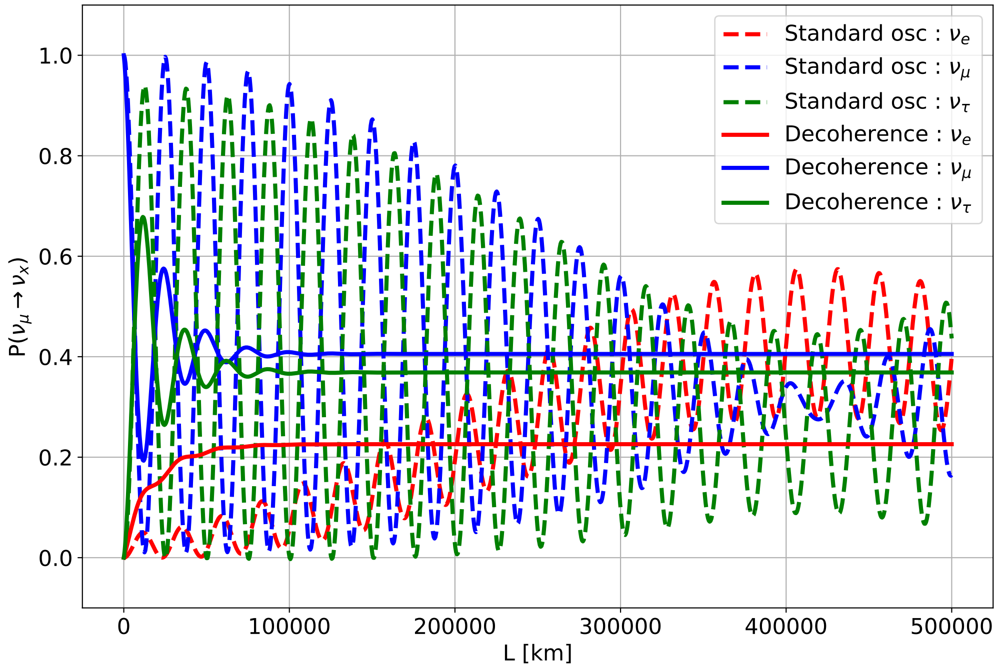

Figure 4.7. – Three-flavor model of neutrino decoherence in vacuum using current best fit values of oscillation parameters from table 2.1 and E_ν = $25GeV$. The decoherence parameters have been set to $\Gamma_{21} = \Gamma_{31} = \Gamma_{32} = 10 feV$.

In reality, atmospheric neutrinos come from at variety of distances and with different energies. Figure 4.8 shows the effects of standard oscillations and decoherence on atmospheric neutrinos at energies and zenith angles relevant to DeepCore, as a function of energy and incoming angle. The direction relates to the cosine of the zenith angle θ_z, where $\cos(\theta_z) = -1$ is an up-going neutrino, meaning that it is coming from the north pole and thus emerges from below the detector travelling upwards. $\cos(\theta_z) = 0$ is a neutrino propagating horizontally with respect to the detector, and $\cos(\theta_z) = 1$ is a down-going neutrino coming from directly above the South Pole (appearing from the south with respect to Earth). The zenith angle is directly related the distance that a neutrino has traveled before interacting.

Two regions of this parameter space are of major interest. Above $50GeV$, muon neutrinos start disappearing in the presence of decoherence. This gives an overall decrease in ν_μ events, correspond to receiving less track-like events in the detector at these energies. The region is in the first oscillations maximum which lies around $25GeV$ at $\cos(\theta_z) = -1$ (widest disappearance band), where muon neutrinos disappearance is weakened compared to the standard oscillation case.

The only difference between a normal or inverted mass ordering is the wiggles appearing at long baselines below $10GeV$. These are created by interactions between electron neutrinos scattering off electrons inside the Earth, known as the Mikheyev-

Smirnov-Wolfenstein (MSW) effect [29]. The MSW effect is sensitive to Δ_m^2, which gets the opposite sign in an inverted mass ordering.

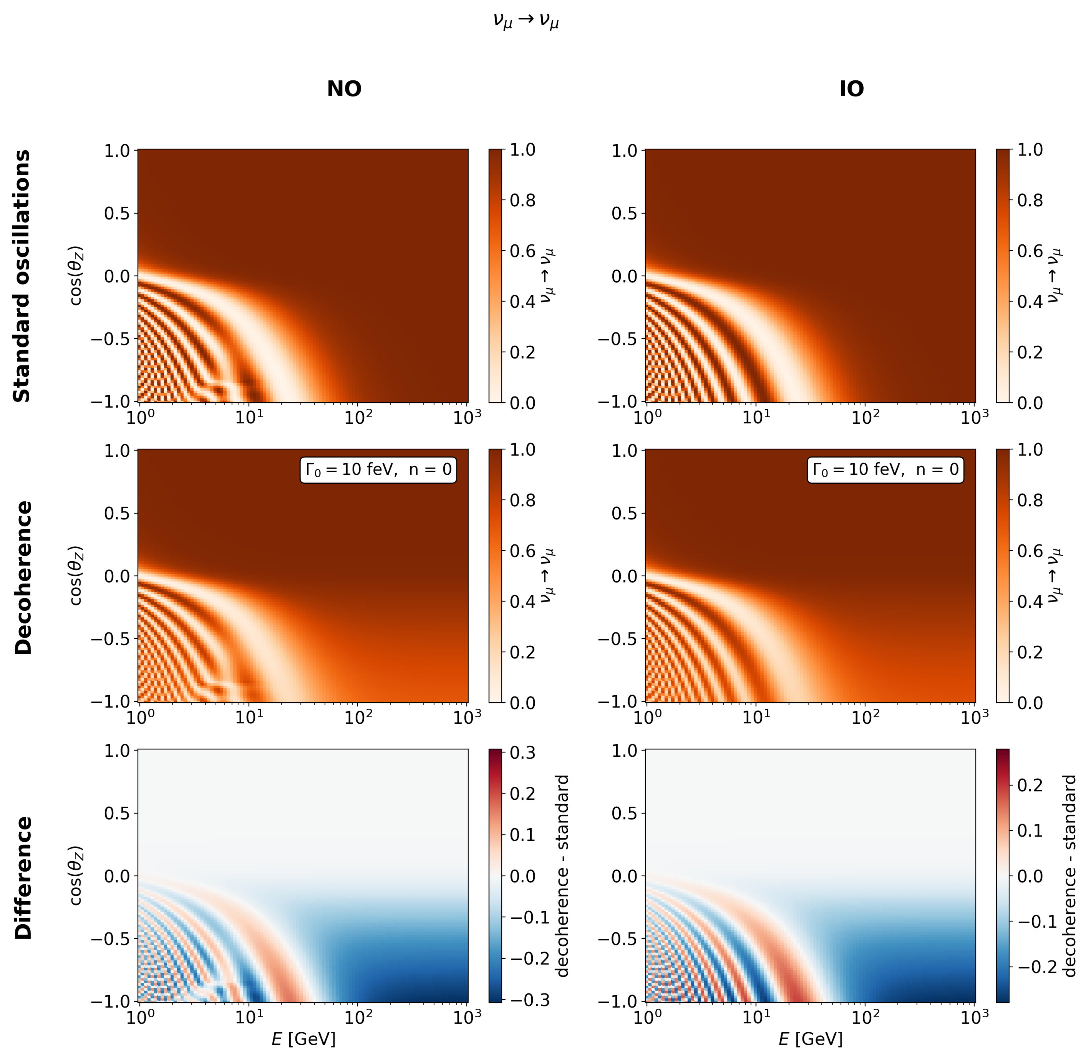

Figure 4.8. – Oscillograms showing the difference between standard oscillations and decoherence for a normal and inverted mass ordering, as a function of incoming angle and energy.

The oscillograms for $\nu_\mu \to \nu_\mu$ shown here as this is the dominant channel for atmospheric neutrinos. The energy dependence ($n = 0$) is included for consistency. Other oscillograms are displayed in appendix A

5 Measuring decoherence with IceCube/DeepCore

With the theoretical framework in place, measuring decoherence can be considered. The analysis technique used is known as a forward folding parameter estimation, in which a template is generated according to different hypotheses and then compared to pseudodata. A truth model is generated from simulation and applied detector response, oscillations, flux corrections, and statistical fluctuations. It is then compared to the data observed by the detector, or in this case pseudodata generated from simulation. Sensitivity to a physics parameter (Γ_0 here) can be calculated by fitting the pseudodata with templates containing various values for the physics parameter, and comparing the fit result to a fit where the physics parameter is allowed to float freely. The details will be explained in section 5.6.

The energy range explored has been chosen to match a realistic analysis with IceCube/DeepCore. For this reason it has been limited to $200\,GeV$, as this energy range has the best data to monte carlo agreement. The analysis will assume that neutrinos have a normal mass ordering, but could be done for both mass orderings.

5.1 The optimal detector

Luckily, cosmic rays are the cause of more than just noise in the detector. The cosmic ray interactions in the atmosphere also create neutrinos. In fact, most of the muon neutrinos observed in IceCube are the product of these. The benefit of looking at neutrinos coming from cosmic rays is that the distance traveled is known, and depends on the incoming angle of the particle detected. This is a huge advantage, as the decoherence effect becomes increasingly visible with distance traveled, as a longer path means passing through more "environment" and thus increases the probability for a perturbation of the wave function. It can be seen in figure 5.1 how a neutrino created near the north pole has a different incoming angle, and for that reason travels longer before reaching the detector, than a neutrino created close to the equator.

It is tempting to use neutrinos of astrophysical origin for the decoherence search, as the distance they travel far exceeds atmospheric neutrinos. But astrophysical neutrinos have some unknowns that make them unqualified for decoherence searches. The precise creation point, and thus the distance traveled before reaching Earth is unknown. This makes us unable to calculate the probability of detecting a specific flavor. Furthermore the flux of astrophysical neutrinos is not known accurately. This limits the ability to estimate how many neutrinos that are expected at certain energies and incoming angles.

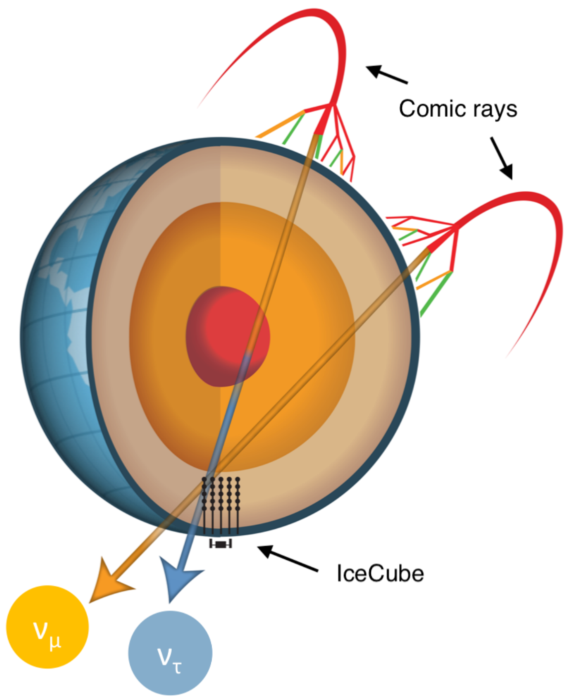

Figure 5.1. – Illustration of how different incoming angles in the detector leads to a difference in distance traveled. One of the neutrinos have oscillated into another flavor along the way.

IceCube has the longest possible baseline achievable on Earth when neutrinos are directly upgoing in the detector. The variety of possible baselines gives an advantage over experiments with a fixed baseline, such as reactor and accelerator experiments. This gives the opportunity to test for an increase in decoherence with distance traveled, whereas only a set increase or decrease in flux can be measured if the baseline is fixed. In the case of a fixed baseline a potential decoherence signal is more easily absorbed in other parameters, or confused with other beyond Standard Model effects, that could have a similar impact.

5.2 Hypothesis testing

The investigation of how well decoherence can be measured with IceCube/DeepCore, happens through hypothesis testing, which is a measure for how much better or worse the data is fitted by a new model, compared to the existing one. The data can be described by a hypothesis that depends on a variety of free parameters, which in this case are fit to match the data with the maximum likelihood method. The likelihood of a function $F(x_i, \vec{p})$ [30] depending on the data x_i and the parameters $\vec{p}$ is given by

$$\mathcal{L}(x, \vec{p}) \quad = \quad \prod_i F(x_i, \vec{p}), \tag{5.1}$$

where $\prod_i$ is the product of all data points in the data a hypothesis is fitted to. The better fit is then given by the hypothesis that maximizes the likelihood value. The product in eq. 5.1 will often be a very tiny number when considering many data points. It can be advantageous to take the natural logarithm on both sides of the equation, to avoid computational issues:

$$\ln \mathcal{L}(x,\vec{p}) = \ln \prod_i F(x_i,\vec{p}) = \sum_i \ln F(x_i,\vec{p}) \tag{5.2}$$

This is known as the Log Likelihood (LLH). The maximum likelihood only tells you which function fits the data better, not how good the fit is. In principle two hypotheses that do not describe the data very well could be tested, and one would still have a higher LLH value.

It can be beneficial to apply a binned LLH comparison when working with large data sets, to decrease the computational time. This is typically done by using the probability mass function of the Poisson distribution

$$\ln \mathcal{L}(\lambda,k)_{binned} = \sum_i \ln F(\lambda,k) \quad , \quad F(\lambda,k) = \frac{\lambda^k}{k!}e^{-\lambda}, \tag{5.3}$$

which gives the probability of observing k number of events in a bin where the truth hypothesis has λ events.

5.2.1 Wilks' theorem

The LLH value can be directly used to get the goodness of fit for an alternative hypothesis compared to the null hypothesis with Wilks' theorem, if the null hypothesis is nested in the alternative model. A nested model is the simpler, containing a subset of the parameters of the alternative. The theorem states that the test statistic

$$-2\Delta LLH = -2\ln\frac{\mathcal{L}(x,\vec{p_0})}{\mathcal{L}(x,\vec{p_1})} \tag{5.4}$$

is χ^2 distributed, with the Degrees of Freedom (DoF) being the difference in number of parameters in p_0 and p_1, when the number of tested hypotheses approaches infinity. The difference in DoFs account for the fact that a superset hypothesis containing more free parameters will always fit the data equally well or better.

The advantage of relating $-2\Delta LLH$ to the χ^2-value is that it allows the conversion to a p-value by using the χ^2 cumulative distribution function (CDF). Evaluating χ^2-CDF with DoF equal to the difference in number of free parameters in the two hypotheses at the value of $-2\Delta LLH$, gives the probability of correctly rejecting the null hypothesis. The conversion from $-2\Delta LLH$ to χ^2 allows the interpretation of how confidently this can be done in terms of 1σ, 90% etc. Figure 5.2 illustrates how a difference in χ^2 can be translated into the probability of correctly rejecting the null hypothesis.

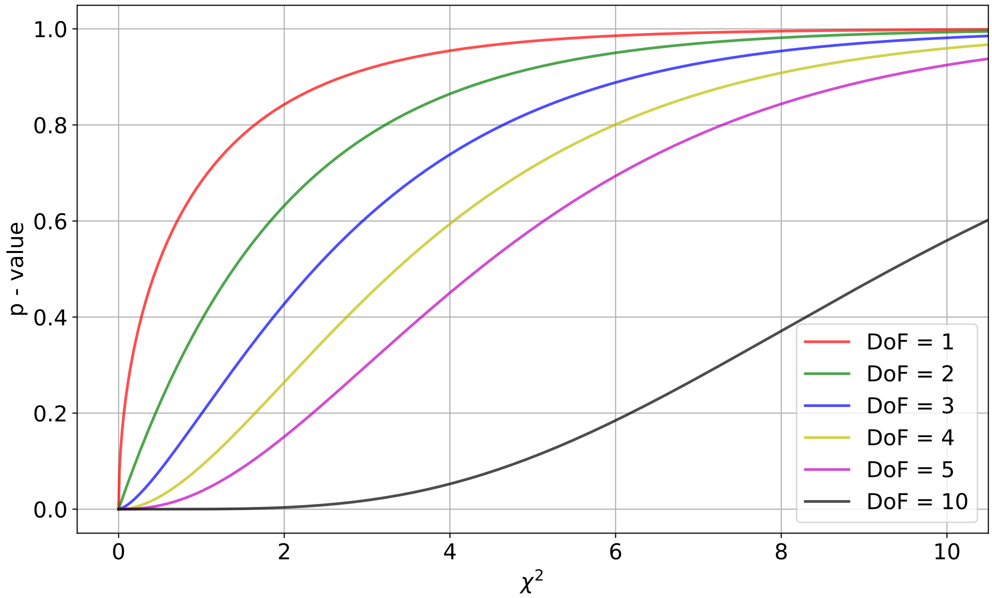

Figure 5.2. – p-value as a function of χ^2 for different degrees of freedom.

5.3 Simulation

The usage of random generated simulation known as Monte Carlo (MC) simulation has become important in modern physics, and has major benefits. One is that a determination of how well we understand the underlying physics of the particles we observe can be made, if it is possible to generate a Probability Distribution Function (PDF) of events from basic assumptions about how likely a neutrino is to interact at different energies, how well the energy and incoming angle is reconstructed, and what the flux is. That must be somewhat understood if simulation agrees with data.

Another benefit is that the analyses can be done "blindly", meaning that the model can be tested on simulation before applying it to real data. In this way results that deviate from the expectation will not affect the analyses, because it is not applied to data until the analyses are completed and checked for errors on simulation. As a result, the final analyses should be less biased due to the lack of knowledge on how changing analyses techniques influence the final results.

In this project MC is used to get an estimated sensitivity to decoherence with IceCube/DeepCore.

5.3.1 Event sample

A sample of neutrino events is required in order to test the decoherence model. This analysis uses pseudodata corresponding to six years of data taking with IceCube/DeepCore. An event sample is selected to maintain the maximum number of neutrinos while getting rid of as much background as possible. The two most important background sources are muons and detector noise, as mentioned in section 3.4.

The event selection used is known as the GeV Reconstructed Events with Containment for Oscillations (GRECO) sample. It is a selection created for a tau neutrino appearance analysis by Michael J. Larson [31]. The selection happens on top of the Simple Multiplicity Trigger, SMT3, which requires 3 HLC hits to occur in DeepCore within a time span of $2.5\mu s$. An event ratio of around 70000 muons per neutrino remains after the SMT3, plus additional background events from noise randomly fulfilling the SMT3 criteria, both of which has to be filtered to get a purer neutrino sample.

A number of different cuts are applied before arriving at the final sample of events. After all cuts are applied the sample is predominantly consisting of atmospheric muon neutrinos. The number of neutrinos compared to muons have been increased by a factor of $7 \cdot 10^5$ to around ten neutrinos per muon, with a total number of approximately 10^5 neutrinos left when using six years of (pseudo) data.

5.4 Degeneracy in Γ parameters

This section continues to use energy independent decoherence where $\Gamma = \Gamma_0$ as an example.

In section 4.3, a decoherence model with only one effective parameter $\Gamma = \Gamma_{21} = \Gamma_{31} = \Gamma_{32}$ was used to display the impact expected by due to decoherence. However the three parameters do not necessarily have to take the same value, and can in principle be anything within the surface of the cone defining the physical region of parameter space shown in figure 4.4. Naturally, the following question arise: How well can possible decoherence models be described by the single Γ model where $\Gamma_{21} = \Gamma_{31} = \Gamma_{32}$? If the answer is 'not well', then which parts of the decoherence parameter phase space can we differentiate from each other, when applying the different models?

The three special cases $\Gamma_{21} = \Gamma_{31}, \Gamma_{32} = 0$, $\Gamma_{21} = \Gamma_{32}, \Gamma_{31} = 0$, and $\Gamma_{31} = \Gamma_{32}, \Gamma_{21} = 0$ are compared to the single Γ model and standard oscillations in figure 5.3. Oscillations are never fully damped when one of the three Γ_{ij} parameters have a value of zero. This can be understood from eq. 4.6 and noting that the off-diagonal terms of the density matrix expressed in the mass basis account for oscillations. The off-diagonal elements are where the time-dependent terms are added when calculating oscillation probabilities (see section 2.3). When one Γ_{ij} parameter takes the value of zero, the two off-diagonal terms in the density matrix that are subtracted that parameter will never vanish because the subtracted term is proportional to Γ_{ij} where $\Gamma_{ij} = 0$, and thus some oscillation remains from those two terms being non-zero in the density matrix. The oscillations of the three special cases where one Γ_{ij} parameter is equal to zero is displayed in figure 5.3.

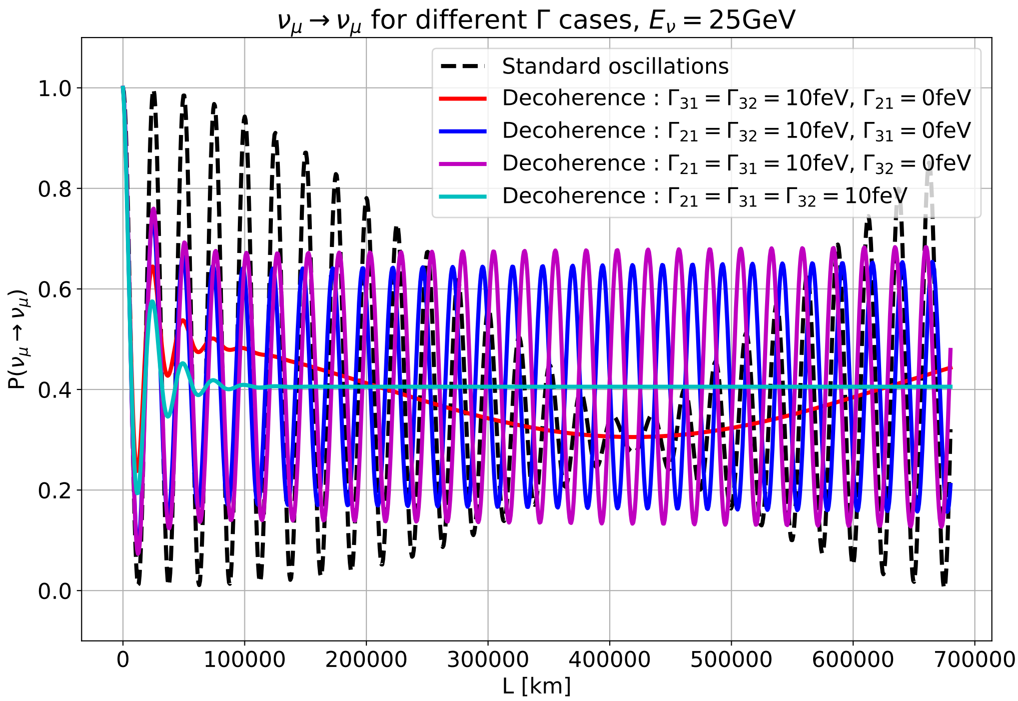

Figure 5.3. – Three-flavor model of neutrino decoherence in vacuum using current best fit values of oscillation parameters from table 2.1 and $E_\nu = 25GeV$. The three special decoherence cases impact on oscillations are shown.

The three cases where one of the Γ_{ij} parameters is set to zero have different impacts on oscillations and are clearly distinguishable at large L. However, this analysis is only sensitive to distances $L \lesssim 12800km$ (since this is the diameter of the Earth), meaning it can be more difficult to tell the difference between models, as the functions describing oscillation probabilities are approximately still in phase.

Figure 5.4 shows the same oscillation probability curves as figure 5.3, but in the distance range relevant for atmospheric neutrinos. The different decoherence models resemble scalable versions of each other. The models described by the blue and purple lines are already qualitatively similar, even without changing any of the parameters. As another example, the model $\Gamma_{21} = \Gamma_{32}$ and $\Gamma_{31} = 0$ (blue line) could be well described by the single Γ model, if the decoherence parameter of the latter took a smaller value. The dashed cyan line displays an alternative model, where the parameters have been tuned to mimic the effect of the model characterized by the solid blue line. The parameter tuning could be done in similar fashion for the other models.

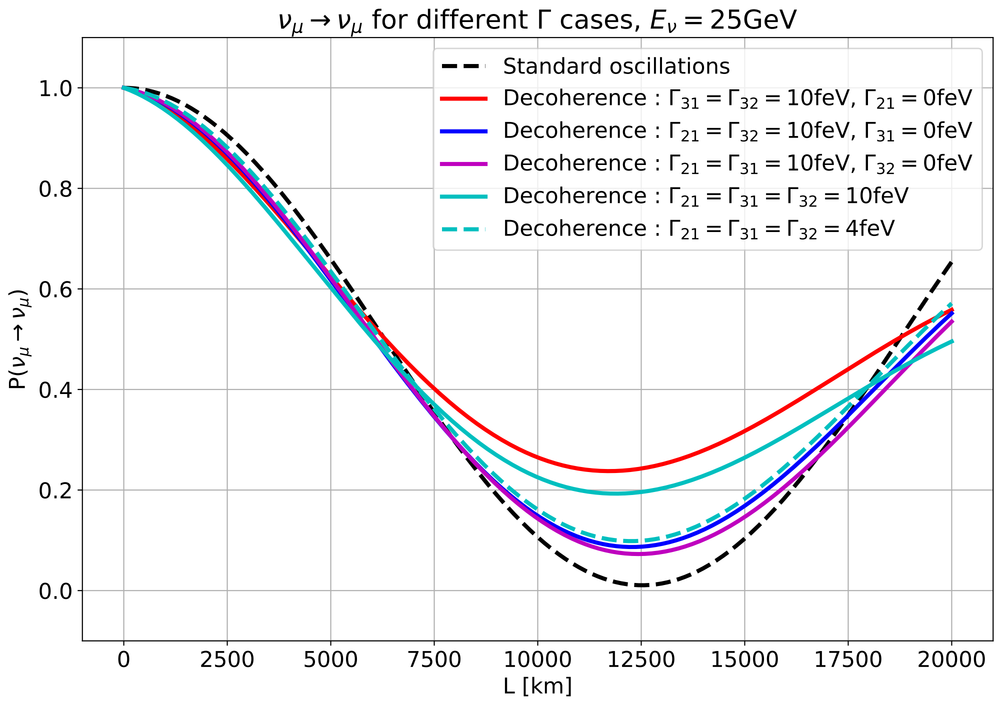

Figure 5.4. – Three-flavor model of neutrino decoherence in vacuum using current best fit values of oscillation parameters from table 2.1 and $E_\nu = 25 GeV$. The different decoherence models can give a similar probability due to the degeneracy of Γ parameters.

This suggest that a wide range of decoherence parameter space could potentially be well described by a single effective Γ parameter, in a search limited to atmospheric neutrinos. In other words, there seems to be some degeneracy in the decoherence parameter space.

An estimation of how well different models can be describe by the single Γ model is visualized in figure 5.5. Random decoherence models have been generated within the allowed Γ parameter space and then fitted with a $\Gamma = \Gamma_{21} = \Gamma_{31} = \Gamma_{32}$ hypothesis. Each point is color-coded according to how well that model can be described by the single Γ hypothesis, in terms of σ. The purpose of this test is to visualize the degeneracy between the Γ_{ij} parameters themselves, and every other parameter/systematic is fixed in the fitting for that reason. In a realistic scenario, the uncertainty in other oscillation parameters, as well as systematic uncertainty, would reduce the ability to differentiate between different decoherence models, if these are freely floating variables in the fitting process. This would increase the degeneracy and thus further motivates the use of a single effective decoherence parameter. The pull of free parameters during the fit of decoherence models will be discussed further in 5.7.1.

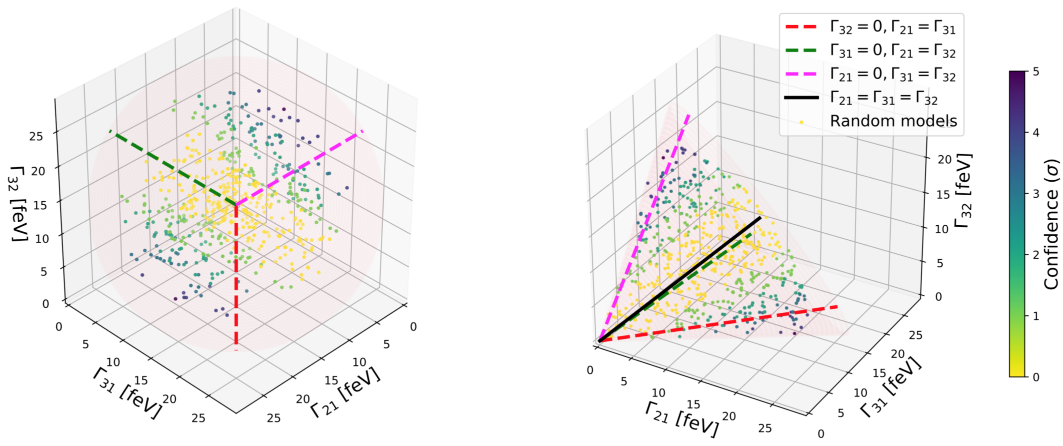

(a) **(b)**

Figure 5.5. – Different decoherence models plotted in decoherence parameter phase space. The color shows how well they are described by a single Γ hypothesis. The same plot is shown at two different rotations.

Figure 5.5 reveals the fact that the degeneracy does not fall off as a function of distance to the single Γ hypothesis. Instead, the degenerate models are distributed in a band around the plane where $\Gamma_{21} = \Gamma_{32}$. If all of the Γ_{ij} parameters are below $5feV$, every model can be described well by the single Γ hypothesis when fitting.

The models have also been compared to a hypothesis without decoherence to explore the discriminating power for decoherence in any form. As seen in figure 5.6, every decoherence model is more distinguishable from standard oscillations already at a few feV, than from the single Γ hypothesis. IceCube is able to differentiate between the decoherence and standard oscillations, if decoherence is a real effect with parameter values larger than a few feV, just by applying the single Γ model. For this reason the applied model will be one containing a single Γ parameter in the rest of this project. The concern about which model is the correct one can be reconsidered, if a decoherence signal is eventually discovered.

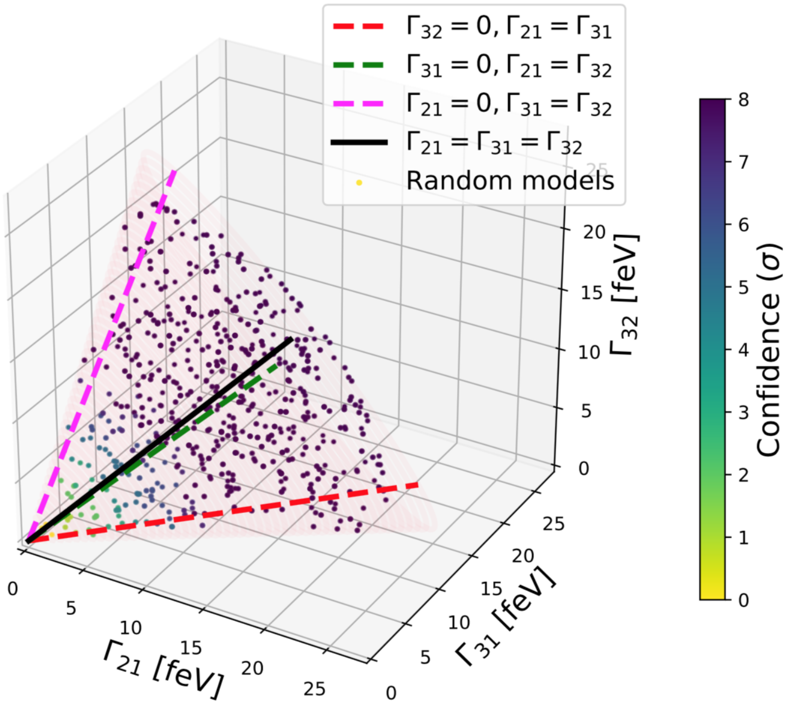

Figure 5.6. – Difference in σ when fitting a no decoherence hypothesis with a random (but allowed) decoherence model.

5.5 Event templates

The oscillograms displayed in figure 4.8 show how a decoherence effect looks in an idealized world without considering statistical fluctuations, event misidentification, imperfect reconstruction, noise, and systematic uncertainties. But the real world is always more complicated. Figure 5.7 shows how the difference between standard oscillations and decoherence would look in number of tracks and cascades detected, as a function of incoming angle and energy. What is seen in the templates depends not only on the parameters listed in section 5.7, but also on how the neutrino flux varies with energy and incoming angle, efficiency of the detector at different energies and angles, and the cross section of different neutrino flavors.

The comparison of standard oscillations and decoherence is stated as statistical significance in terms of the difference in bin content in such templates.

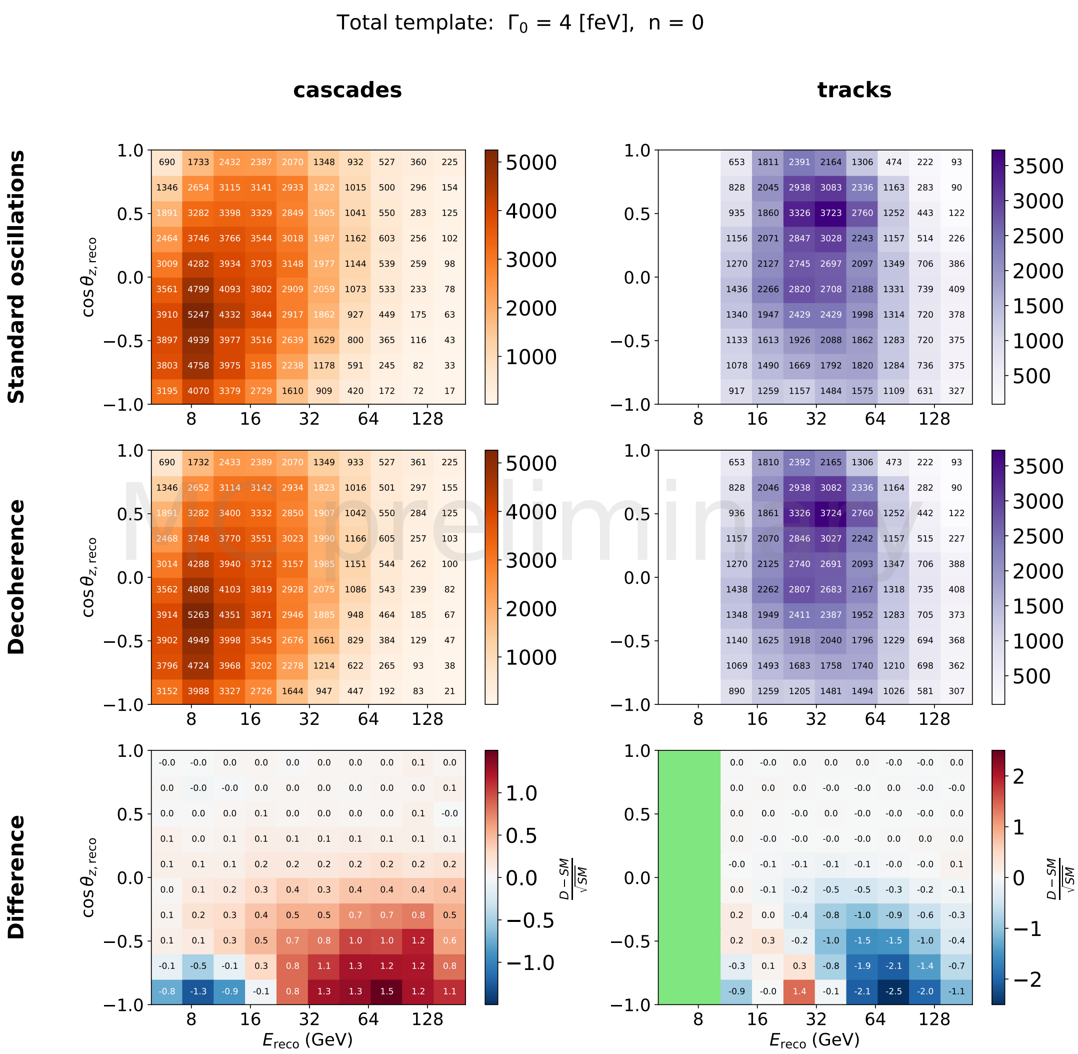

Figure 5.7. – Number of events per bin as function of reconstructed energy and zenith angle. The decoherence model used is the single Γ model with $\Gamma_0 = 4feV$, corresponding to the strength required for a 5σ discovery potential when using IceCube/DeepCore.

5.6 Sensitivity test for energy independent decoherence

Determining the estimated sensitivity to decoherence in IceCube/DeepCore is done by comparing the event templates described in the previous section, which are generated according to different hypotheses. The estimated sensitivity to decoherence is obtained in the following way:

Pseudodata is generated according to some hypothesis. The could be either one without decoherence ($\Gamma = 0$) or with an injected signal ($\Gamma = const$). The generated pseudodata is then fit using the binned maximum likelihood method, with a template where the physics parameter, Γ, is allowed to float.

A number of alternative hypotheses are generated for the sensitivity scan, with Γ fixed to different values, each of which are minimized to fit the pseudodata as well as possible. The difference in LLH between the free fit with Γ floating and the scanned point (where Γ is fixed to the scanned value) is then calculated. The -2ΔLLH can then be translated to the significance at which the scanned point can be excluded using Wilks' theorem. Note again that $\Gamma_0 = \Gamma$ when the model is energy independent ($n = 0$, see eq. 4.7), and Γ will be used throughout this section. The plots in figure 5.8 and 5.9 are generated using asimov pseudodata, meaning without statistical fluctuations.

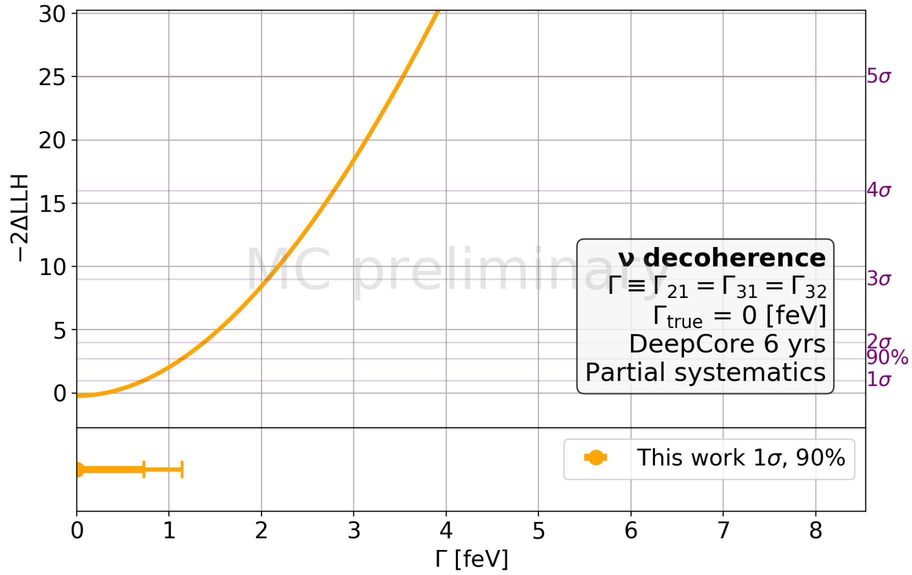

Figure 5.8. – Asimov sensitivity test using pseudodata with $\Gamma_{true} = 0$ and $n = 0$.

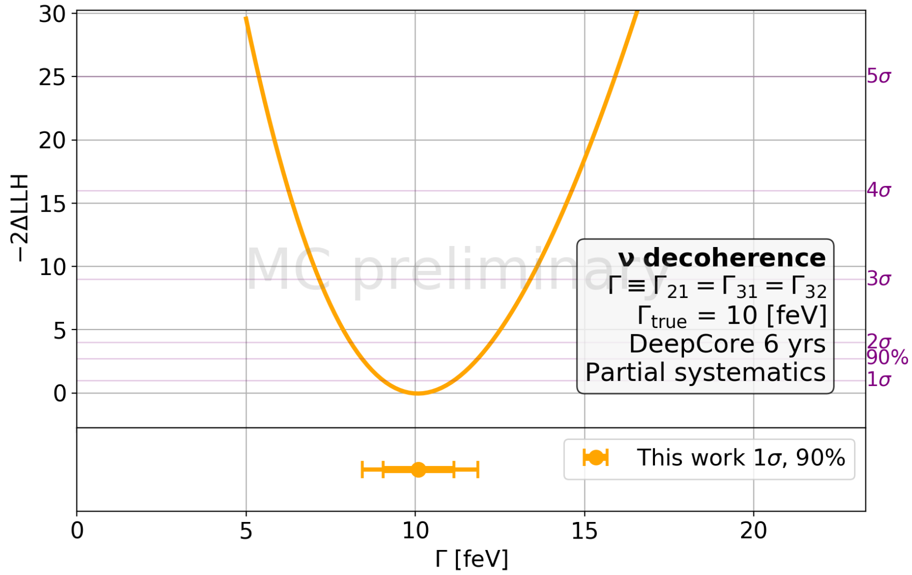

Figure 5.9. – Asimov sensitivity test using pseudodata with $\Gamma_{true} = 10 feV$ and $n = 0$.

Figure 5.8 shows the sensitivity in IceCube in the case of the pseudodata being generated without decoherence ($\Gamma_{true} = 0$). The -2ΔLLH value and the corresponding significance in standard deviations is displayed as a function of the value that the physics parameter Γ takes. A case with pseudodata including decoherence at a strength of $\Gamma_{true} = 10feV$ is displayed in figure 5.9.

The case of a decoherence measurement is included here to display how it compares to making an upper limit. The rest of the project will take the slightly pessimistic approach where decoherence is not currently measurable with IceCube/DeepCore, and thus only display the estimated upper limits (no more injections of decoherence signal).

A real measurement would be subject to statistical fluctuations in data. For this reason the sensitivity test in figure 5.10 has been repeated 200 times, each with fluctuations applied to the pseudodata. The figure displays confidence intervals; that is the intervals within which the -2ΔLLH took a value in 68% and 90% of the tests.

The scan points around 0 take a negative -2ΔLLH value, implying that points with $\Gamma \neq 0$ fit the pseudodata better than the test where Γ was floating freely. This can happen in cases where the minimizer does not find the global minimum in the free fit, because the extra free parameter has complicated the LLH space.

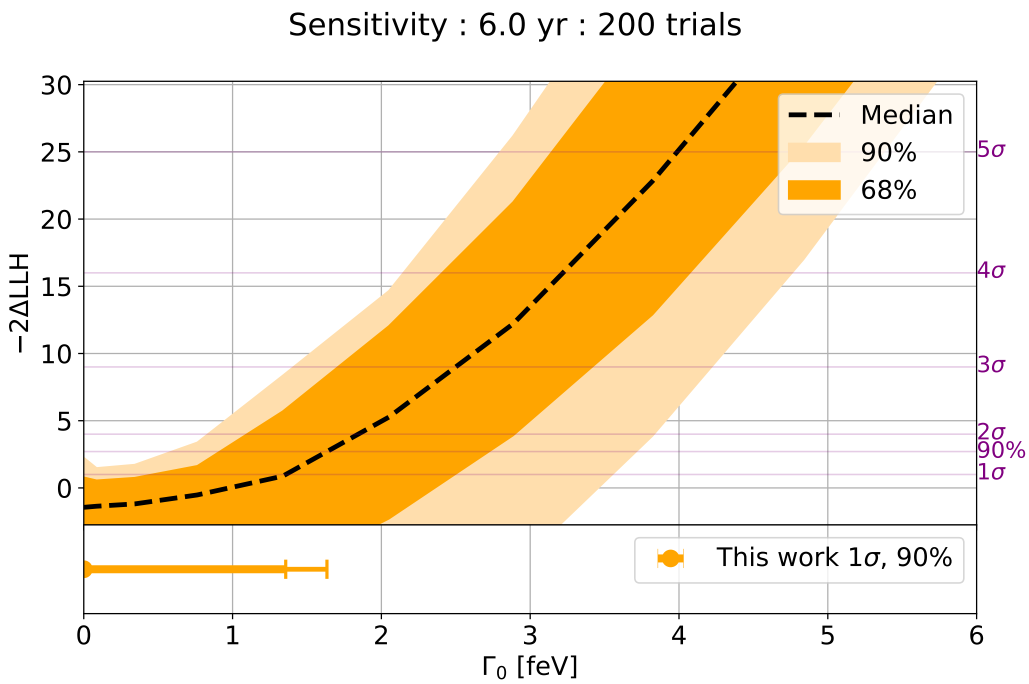

Figure 5.10. – Sensitivity to decoherence, using pseudodata generated with $\Gamma_{true} = 0$ and $n = 0$. The confidence intervals are made by displaying the area that 68% and 90% of the trials fit within.

The sensitivity to decoherence characterized by a single energy independent Γ parameter is found, by evaluating the median at desired statistical significances. Using IceCube/DeepCore Γ can be limited to

$$\Gamma \quad \leq \quad 1.4(1.6)[feV] \quad at \quad 68\%(90\%) \quad CL, \tag{5.5}$$

in the case of energy independent decoherence.

5.7 Fit parameters

The Minimization process in the sensitivity test is performed with a number of free parameters, which are fitted to minimize the difference in likelihood between the hypotheses with various fixed Γ, and the one where Γ is floating freely. The free parameters in the fit are listed in table 5.1.

Parameter	Description
$\frac{\nu_e}{\nu_\mu}$	Flux ratio of ν_e and ν_μ with respect to nominal value
Barr uphor ratio	Flux ratio of horizontal and upgoing neutrinos
Barr $\frac{\nu}{\bar{\nu}}$	Flux ratio of neutrinos and anti-neutrinos
δ index	Correction to spectral index of neutrino the flux: $\Phi_\nu \propto E^{-k+\delta}$
$\delta\gamma_\mu$	Correction to spectral index of the muon flux: $\Phi_\mu \propto E^{-k+\delta}$
θ_{23}	Atmospheric mixing angle
Δm^2_{31}	ν_1 and ν_3 mass difference squared
GENIE Ma QE	Cross section parameter for QE
GENIE Ma RES	Cross section parameter for RES
Effective scale	Scaling parameter for the total neutrino rate
Weight scale	Scaling parameter for the total muon rate
ν_τ normalization	Scaling parameter for the ν_τ and $\bar{\nu_\tau}$ rates
ν_{NC} normalization	Scaling parameter for the NC rates

Table 5.1. – Free parameters in the fits performed during sensitivity tests. Some flux uncertainties are named Barr after the author of a flux uncertainty paper from 2006 [32].

There are a few benefits to implementing some of the flux parameters as ratios: The minimizer has less free parameters which makes the process faster, and some of the uncertainties cancel when the ratio is taken. An example of this is illustrated in the Barr paper [32], where the uncertainty of $\frac{\nu_e}{\nu_\mu}$ is generally a factor 3 to 5 lower than the uncertainty of $\frac{\nu_e}{\bar{\nu_e}}$ or $\frac{\nu_\mu}{\bar{\nu_\mu}}$.

Some parameters are fixed in the fitting process, due to the lack of importance to the analysis, for example Δm^2_{21} and the distance above earth that neutrinos are generated. The impact that the fixed parameters has on the analysis have been checked in a fit where they were allowed to float freely. Parameters that have little or no impact are fixed to lower computational time and reduce complexity of the LLH-space, making it easier for the minimizer to find the correct global minimum.

5.7.1 Parameter pulls

The parameters that are floating freely during the fitting process are not always fit back to the values that the pseudodata is generated from. The free parameters in a sensitivity test can pull in certain directions, to compensate for the fact that an incorrect hypothesis is fitted. The parameters can take different values to make the decoherence template more similar to the truth template. The pull of individual parameters can be seen in figure 5.11.

Six parameters are significantly different from their value in the truth template; $\frac{\nu_e}{\nu_\mu}$, Barr $\frac{\nu}{\bar{\nu}}$, Effective scale, ν_τ normalization, ν_{NC} normalization, and Weight scale. The effect of a combined parameter pull is non-trivial. As an example, the $\frac{\nu_e}{\nu_\mu}$ moves towards higher values with increasing Γ_0, which increases the overall number of cascades. On the other hand the ν_{NC} normalization is pulled to lower values, decreasing the number of cascades. The two parameters could have slightly different impacts in distinct regions of the template, making the combined effect of all the parameter pulls lower the impact that a decoherence parameter has on the template.

It is also worth noting that θ_{23} increasingly favors a value above $45°$ with larger Γ_0 values.

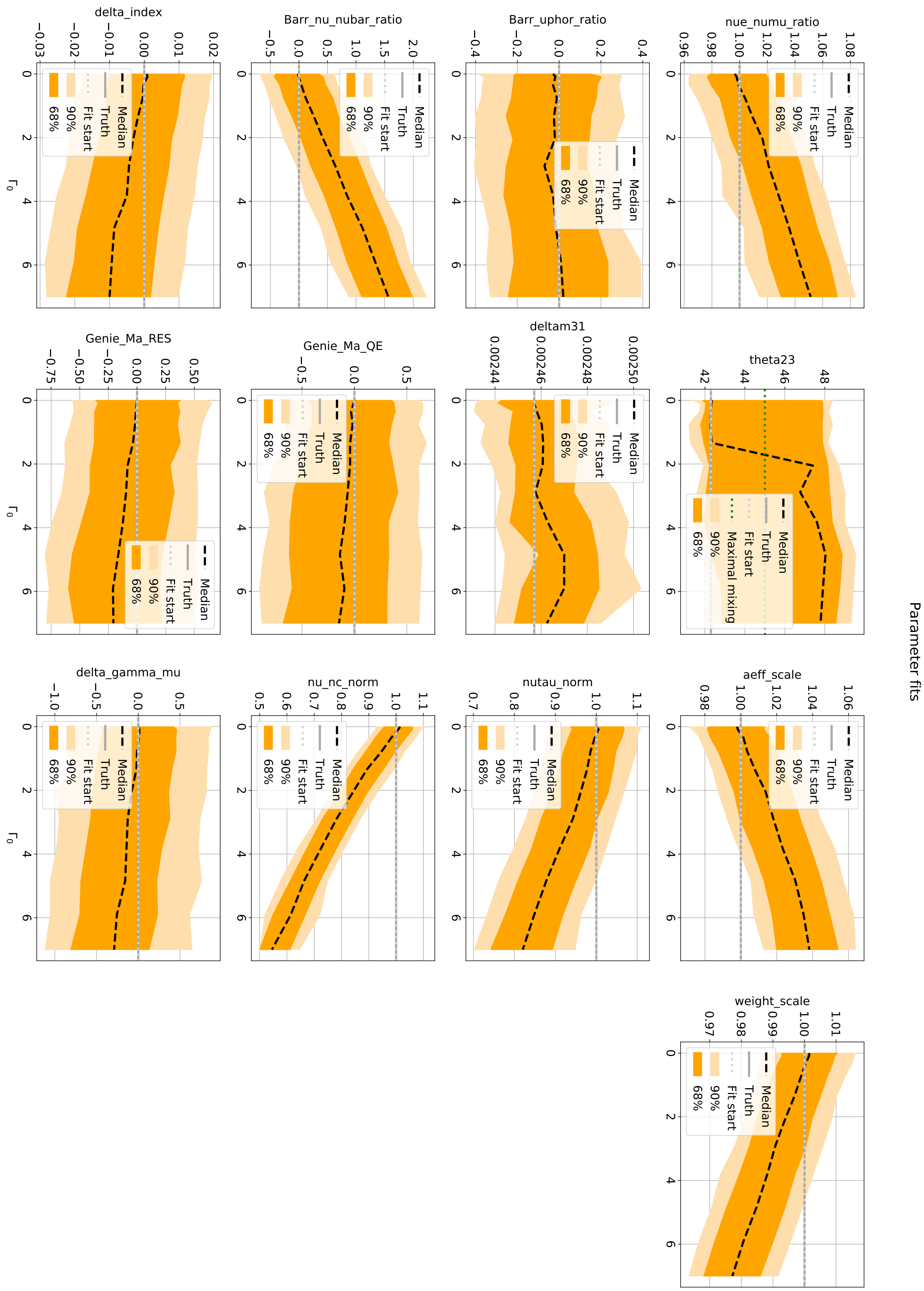

Figure 5.11. – The value that each free parameter is fitted to, as a function of Γ_0. The contours are made from 200 trials of statistically fluctuated templates

5.8 Energy dependent decoherence

The possibility for decoherence to be energy dependent is motivated by some quantum gravity models [33], which predicts that $\Gamma \propto \Gamma_0 E^2$. Even without the motivation quantum gravity models, one could imagine that the probability of interacting in the neutrino mass basis scales with energy, just like it does with weak interactions. Energy dependent decoherence follows the formulation from section 4.2.1, where n is the index of a power law describing the energy dependence. It is important to remember the difference between Γ and Γ_0 in the energy dependent cases, which can be reviewed in section 4.2.1.

5.8.1 n = 2

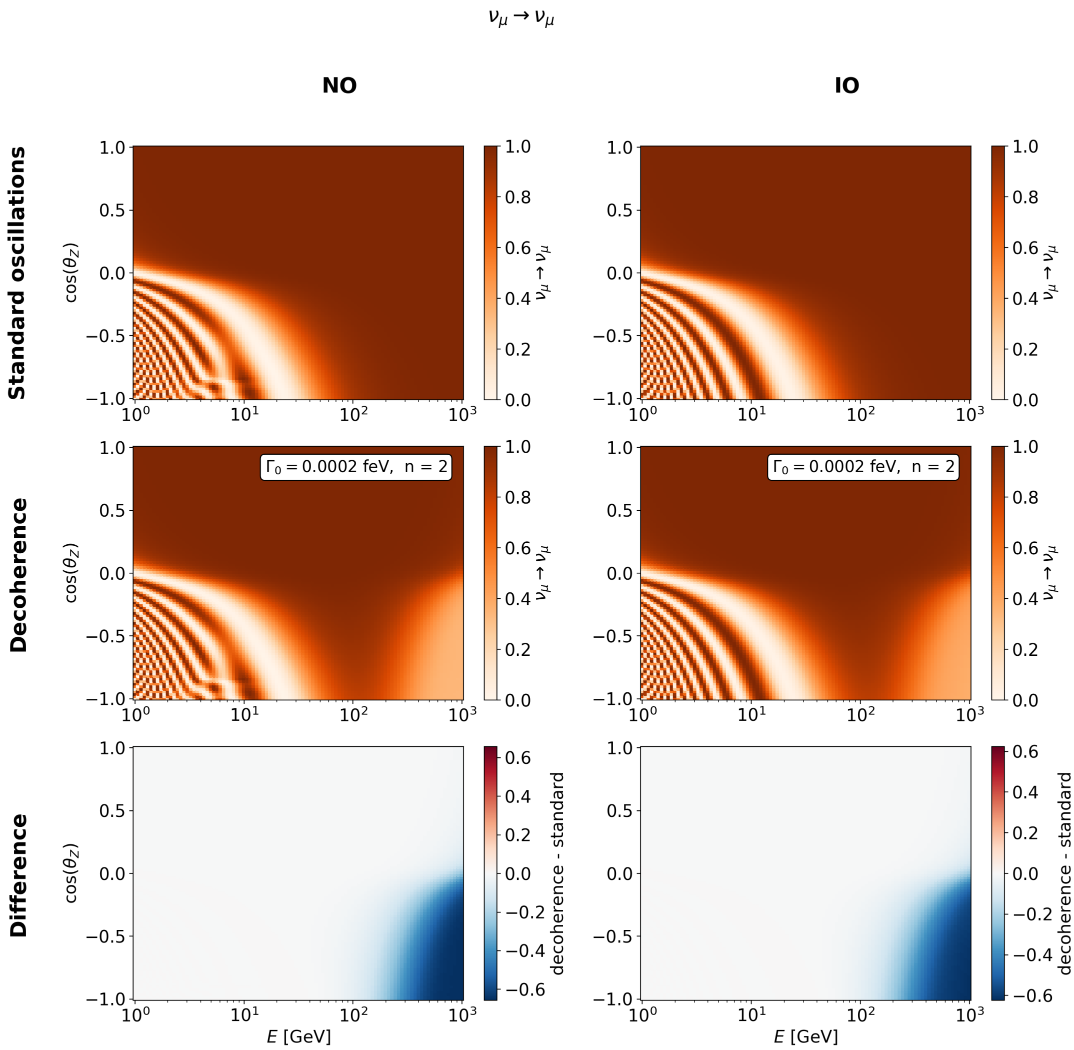

Figure 5.12. – Oscillograms showing the difference between standard oscillations and decoherence for a normal and inverted mass ordering, as a function of incoming angle and energy. The oscillograms are generated using $\Gamma_0 = 200 zeV$ the $n = 2$ energy dependence.

The energy dependent decoherence model with $n = 2$ will be considered here as an example, but the same analysis was also done for models with $n = -2, -1$, and 1, to get the upper limits in each case. The impacts that decoherence have on neutrino oscillations are different, when applying an energy dependent model. Figure 5.12 shows the oscillogram when considering the $n = 2$ case. A value of $\Gamma_0 = 200 zeV$ is used here (which corresponds to the estimation of where a 5σ discovery potential would be using IceCube/DeepCore in the $n = 2$ case), as the decoherence effect becomes more significant when considering an energy dependence with a positive n.

The effective Γ parameter now take a much higher value at large E_ν, and increases with energy from $200 zeV$ for neutrinos with $E_\nu = 1 GeV$ to $200 feV$ for neutrinos with $E_\nu = 1 TeV$.

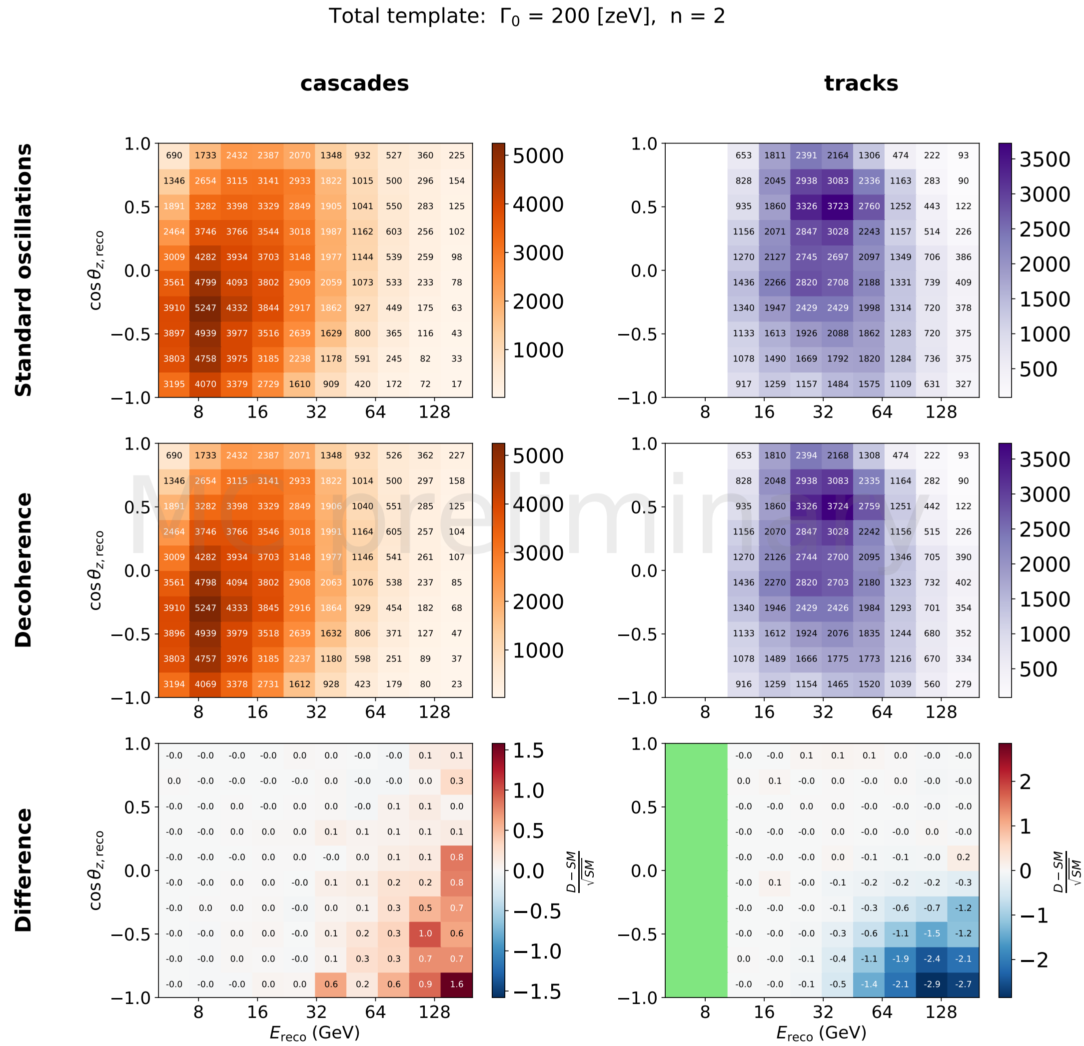

Figure 5.13. – Number of events per bin as function of reconstructed energy and zenith angle. The decoherence model used is the single Γ model with $\Gamma_0 = 200 zeV$, corresponding to the strength required for a 5σ discovery potential when using IceCube/DeepCore.

The MC templates displayed in figure 5.13 are only affected at higher energies in this case, as the effective Γ value is below $1 feV$ at energies below $\sim 70 GeV$.

The sensitivity to different energy dependent decoherence models can be estimated in the same way as with the energy independent decoherence model considered in section 5.6. This gives an upper limit for the strength of Γ_0 that is dependent on n. The sensitivity to Γ_0 for $n = 2$ can be seen on figure 5.14

Figure 5.14. – Sensitivity to decoherence using pseudodata generated with $\Gamma_0 = 0$ and $n = 2$. The confidence intervals are made by displaying the area that 68% and 90% of the trials fit within.

5.8.2 Upper limits for different *n*

The upper limits to five different energy dependent decoherence models where $n \in [-2, -1, 0, 1, 2]$ have be calculated with sensitivity tests. The sensitivity curves for n cases that have not been displayed previously are shown in appendix B. Figure 5.15 displays the upper limits on Γ_0 for different cases of energy dependency. The values of each limit are also displayed in table 5.2.

The upper limits on Γ_0 determined for positive n decrease rapidly with n because all of the decoherence signal appears in a region that is not complicated by oscillations. The opposite is true for negative n, because the signal appears in a region with oscillations.

n	68%	90%
-2	$47.4\,feV$	$77.9\,feV$
-1	$9.8\,feV$	$18.2\,feV$
0	$1.4\,feV$	$1.6\,feV$
1	$6.0\,aeV$	$10.3\,aeV$
2	$23.8\,zeV$	$44.4\,zeV$

Table 5.2. – The 68% and 90% upper limits on Γ_0 in five different energy dependent decoherence models.

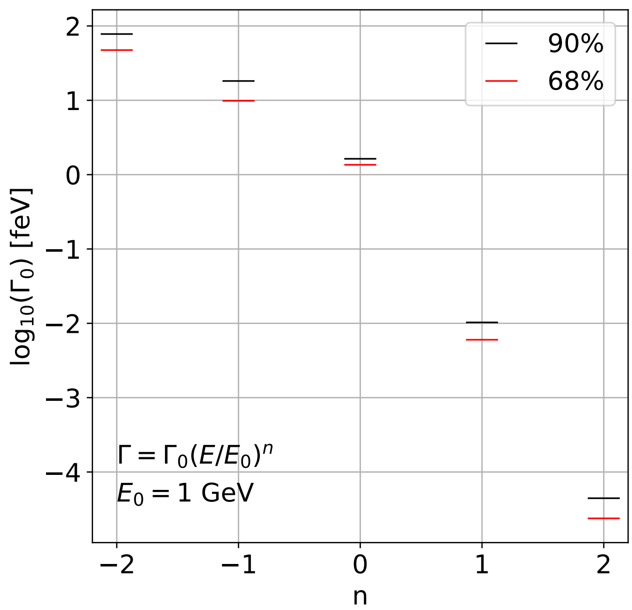

Figure 5.15. – 68% and 90% Confidence levels for five different cases of energy dependence ranging from $n = -2$ to $n = 2$.

5.9 Previous decoherence searches

The original motivation for this project was a disagreement in the measurement of θ_{23} between the two long baseline accelerator experiments NOvA and T2K [35]. The measurement from T2K was favoring maximal mixing ($\theta_{23} = 45°$), whereas NOvA measured θ_{23} to be non-maximal. One of the main difference between the two experiments is their difference in baseline, being $295km$ and $810km$ for T2K and NOvA respectively. It was proposed that the difference in measurements could be caused by neutrino decoherence [34], as it can mimic the effect of less effective mixing. The strength of this decoherence effect would have to be in the order $\sim 20 feV$ to account fully for the discrepancy. The tension was however resolved when the new result from NOvA came out in the beginning of 2018. Both experiments now have maximal mixing included in their 90% confidence level.

A search for decoherence using one year of public IceCube data was carried out in the first half of 2018 [36]. The three special cases where one decoherence parameter take the value of zero are examined in the paper.

A search for decoherence was carried out almost two decades ago, using the Super Kamiokande detector [28]. A two neutrino flavor approximation was used in this analysis, which makes the result hard to interpret in a framework using three flavors. However the study gives a rough idea of the range of Γ values a search should investigate.

It was proposed in [37] that decoherence could resolve the LSND anomaly, in which the experiment detected an excess in neutrino events at low energies. The decoherence strength required to explain the anomaly is $\Gamma_0 \sim 1.2 \cdot 10^{11} feV$. For this reason a energy dependent model that makes the signal peak in the desired region is used, as a model without energy dependence would be excluded already.

This study covers a parameter space that has not been explored in previous searches with the exception of [36]. In comparison to [36], a larger statistics sample of IceCube data is used and the parameter space is explored in a different manner. This leaves neutrino decoherence as an open topic with plenty of room for improved searches.

Summary and concluding remarks

6

The theory and phenomenology of a neutrino oscillations model including decoherence as a sub-leading effect is presented in this thesis. Neutrino decoherence arises when treating neutrinos as propagating in an open quantum system, in which they are coupled to the surrounding environment. The implementation of a model containing the combined effects of neutrino oscillations and decoherence has enabled the study of how this dampens oscillations, which alters the probability of observing the different neutrino flavors as a function of energy/distance traveled. The potential for observing decoherence with IceCube is visualized, and both a decoherence toy model and a complete three-flavor model containing the presently known neutrino physics have been investigated.

Neutrino decoherence can be characterized by three parameters; Γ_{21}, Γ_{31}, and Γ_{32}, each of which are limited within a range depending on the values of the other two. The work shown in this thesis support that a model with a single parameter where $\Gamma_{21} = \Gamma_{31} = \Gamma_{32} = \Gamma$ is sufficient to search for a decoherence signal, while models where the three parameters take different values are almost indistinguishable in IceCube.

Neutrino decoherence has been implemented in an IceCube analysis framework to investigate how it would impact the observed data. Estimations of the sensitivity to decoherence with different energy dependencies, where $\Gamma = \Gamma_0\left(\frac{E_\nu}{GeV}\right)^n$, have been calculated using a Monte Carlo simulation of IceCube data. IceCube/DeepCore is sensitive to energy independent decoherence down to $\Gamma \leq 1.6 feV$ (90% CL).

The presented analysis will be applied to real data at a later time, when final checks and implementations have been carried out, and the analysis methods have been reviewed and approved by the IceCube collaboration. Using the IceCube detector for a decoherence analysis can produce world leading upper limits on the decoherence parameters.

6.1 Future work

A couple of tasks need to be carried out before the analysis is ready to be applied to real data. The most important is the inclusion of IceCube detector systematic uncertainties, which includes photon scattering and absorption uncertainties of the ice, and DOM efficiency. The inclusion will allow for a more realistic limit to decoherence. The impact of using detector systematic uncertainties needs to be investigated before the analysis can be carried out in a satisfactory way.

The upper limits to decoherence can be improved by including data at higher energies than $E_\nu > 200 GeV$. This region has the advantage of better angular resolution for tracks, and the benefit of no oscillations. Extending the search to this regions could have other complications though, such as less knowledge of the neutrino origin (atmospheric or astrophysical) and a smaller neutrino flux.

A correlation between decoherence and matter effects for $\Gamma > 1000 feV$ was discovered but not mentioned in this thesis, due to the lack of understand of whether it is a real effect or an effect of incorrect software implementation. This was discovered recently, and needs further investigation.

Bibliography

[1] W. Pauli. "Dear radioactive ladies and gentlemen". In: *Phys. Today* 31N9 (1978), p. 27 (cit. on p. 1).

[2] C. L. Cowan Jr., F. Reines, F. B. Harrison, H. W. Kruse, and A. D. McGuire. *Detection of the Free Neutrino: A Confirmation*. 1956 (cit. on p. 1).

[3] Bruce T. Cleveland, Timothy Daily, Jr. Raymond Davis, et al. "Measurement of the Solar Electron Neutrino Flux with the Homestake Chlorine Detector". In: *The Astrophysical Journal* 496.1 (1998), p. 505 (cit. on p. 1).

[4] *The Standard Model and beyond*. `http://united-states.cern/physics/standard-model-and-beyond` (cit. on p. 2).

[5] M. Tanabashi et al. (Particle Data Group). *Particle Data Group - 2018 Review*. 2018 (cit. on p. 3).

[6] F. Zwicky. "Die Rotverschiebung von extragalaktischen Nebeln". In: *Helv. Phys. Acta* 6 (1933). [Gen. Rel. Grav.41,207(2009)], pp. 110–127 (cit. on p. 3).

[7] Q. R. Ahmad et al. "Measurement of the rate of $\nu_e + d \to p + p + e^-$ interactions produced by ^8B solar neutrinos at the Sudbury Neutrino Observatory". In: *Phys. Rev. Lett.* 87 (2001), p. 071301. arXiv: `nucl-ex/0106015 [nucl-ex]` (cit. on p. 4).

[8] *Chapter 9, Density Matrices*. `http://homepage.univie.ac.at/reinhold.bertlmann/pdfs/T2_Skript_Ch_9corr.pdf` (cit. on pp. 4, 5).

[9] *5.74 Introductory Quantum Mechanics II*. `https://ocw.mit.edu/courses/chemistry/5-74-introductory-quantum-mechanics-ii-spring-2009/lecture-notes/MIT5_74s09_lec12.pdf` (cit. on p. 4).

[10] *Chapter 3, Operator methods in quantum mechanics*. `http://www.tcm.phy.cam.ac.uk/~bds10/aqp/handout_operator.pdf` (cit. on p. 5).

[11] B. Pontecorvo. "Inverse beta processes and nonconservation of lepton charge". In: *Sov. Phys. JETP* 7 (1958). [Zh. Eksp. Teor. Fiz.34,247(1957)], pp. 172–173 (cit. on p. 9).

[12] Ziro Maki, Masami Nakagawa, and Shoichi Sakata. “Remarks on the Unified Model of Elementary Particles”. In: *Progress of Theoretical Physics* 28.5 (1962), pp. 870–880 (cit. on p. 9).

[13] Ivan Esteban, M. C. Gonzalez-Garcia, Michele Maltoni, Ivan Martinez-Soler, and Thomas Schwetz. “Updated fit to three neutrino mixing: exploring the accelerator-reactor complementarity”. In: *JHEP* 01 (2017), p. 087. arXiv: `1611.01514 [hep-ph]` (cit. on p. 10).

[14] A. Bellerive, J. R. Klein, A. B. McDonald, A. J. Noble, and A. W. P. Poon. “The Sudbury Neutrino Observatory”. In: *Nucl. Phys.* B908 (2016), pp. 30–51. arXiv: `1602.02469 [nucl-ex]` (cit. on p. 11).

[15] *Juno*. `http://www.staff.uni-mainz.de/wurmm/juno.html` (cit. on p. 11).

[16] *Official IceCube webpage*. `https://icecube.wisc.edu/` (cit. on p. 12).

[17] R. Abbasi et al. “The Design and Performance of IceCube DeepCore”. In: *Astropart. Phys.* 35 (2012), pp. 615–624. arXiv: `1109.6096 [astro-ph.IM]` (cit. on p. 12).

[18] M. G. Aartsen et al. “The IceCube Neutrino Observatory: Instrumentation and Online Systems”. In: *JINST* 12.03 (2017), P03012. arXiv: `1612.05093 [astro-ph.IM]` (cit. on p. 13).

[19] “Neutrino emission from the direction of the blazar TXS 0506+056 prior to the IceCube-170922A alert”. In: *Science* 361.6398 (2018). Ed. by Mark Aartsen, Markus Ackermann, and Adams, pp. 147–151. eprint: `http://science.sciencemag.org/content/361/6398/147.full.pdf` (cit. on p. 14).

[20] J. A. Formaggio and G. P. Zeller. “From eV to EeV: Neutrino Cross Sections Across Energy Scales”. In: *Rev. Mod. Phys.* 84 (2012), pp. 1307–1341. arXiv: `1305.7513 [hep-ex]` (cit. on p. 15).

[21] M. J. Larson. “Simulation and identification of non-Poissonian noise triggers in the IceCube neutrino detector”. PhD thesis. Alabama U., 2013 (cit. on p. 17).

[22] David Heereman von Zuydtwyck. “HitSpooling: an improvement for the supernova neutrino detection system in icecube”. PhD thesis. University Libre, Brussels, 2015 (cit. on p. 18).

[23] Patrignani C. et al. “Review of Particle Physics”. In: *Chin. Phys.* C40.10 (2016), p. 100001 (cit. on p. 19).

[24] Steven B. Giddings and Andrew Strominger. “Loss of incoherence and determination of coupling constants in quantum gravity”. In: *Nuclear Physics B* 307.4 (1988), pp. 854 –866 (cit. on p. 20).

[25] John Ellis, John S. Hagelin, D.V. Nanopoulos, and M. Srednicki. “Search for violations of quantum mechanics”. In: *Nuclear Physics B* 241.2 (1984), pp. 381 –405 (cit. on p. 20).

[26] G. Lindblad. "On the generators of quantum dynamical semigroups". In: *Comm. Math. Phys.* 48.2 (1976), pp. 119–130 (cit. on p. 23).

[27] Philip Pearle. "Simple Derivation of the Lindblad Equation". In: *European Journal of Physics* 33.4 (2012), p. 100001. arXiv: `1204.2016 [math-ph]` (cit. on p. 24).

[28] E. Lisi, A. Marrone, and D. Montanino. "Probing possible decoherence effects in atmospheric neutrino oscillations". In: *Phys. Rev. Lett.* 85 (2000), pp. 1166–1169. arXiv: `hep-ph/0002053 [hep-ph]` (cit. on pp. 26, 50).

[29] A. Yu. Smirnov. "The MSW effect and matter effects in neutrino oscillations". In: *Phys. Scripta* T121 (2005), pp. 57–64. arXiv: `hep-ph/0412391 [hep-ph]` (cit. on p. 30).

[30] R. A. Fisher. *On the mathematical foundations of theoretical statistics*. 1922 (cit. on p. 32).

[31] M. J. Larson. "A Search for Tau Neutrino Appearance with IceCube-DeepCore". PhD thesis. Copenhagen U., 2018 (cit. on p. 35).

[32] G. D. Barr, T. K. Gaisser, S. Robbins, and Todor Stanev. "Uncertainties in Atmospheric Neutrino Fluxes". In: *Phys. Rev.* D74 (2006), p. 094009. arXiv: `astro-ph/0611266 [astro-ph]` (cit. on pp. 43, 44).

[33] John R. Ellis, N. E. Mavromatos, Dimitri V. Nanopoulos, and Elizabeth Winstanley. "Quantum decoherence in a four-dimensional black hole background". In: *Mod. Phys. Lett.* A12 (1997), pp. 243–256. arXiv: `gr-qc/9602011 [gr-qc]` (cit. on p. 46).

[34] JoÃčo A. B. Coelho and W. Anthony Mann. "Decoherence, matter effect, and neutrino hierarchy signature in long baseline experiments". In: *Phys. Rev.* D96.9 (2017), p. 093009. arXiv: `1708.05495 [hep-ph]` (cit. on p. 49).

[35] Joao A. B. Coelho, W. Anthony Mann, and Saqib S. Bashar. "Nonmaximal θ_{23} mixing at NOvA from neutrino decoherence". In: *Phys. Rev. Lett.* 118.22 (2017), p. 221801. arXiv: `1702.04738 [hep-ph]` (cit. on p. 49).

[36] Pilar Coloma, Jacobo Lopez-Pavon, Ivan Martinez-Soler, and Hiroshi Nunokawa. "Decoherence in Neutrino Propagation Through Matter, and Bounds from IceCube/DeepCore". In: (2018). arXiv: `1803.04438 [hep-ph]` (cit. on p. 50).

[37] Pouya Bakhti, Yasaman Farzan, and Thomas Schwetz. "Revisiting the quantum decoherence scenario as an explanation for the LSND anomaly". In: *JHEP* 05 (2015), p. 007. arXiv: `1503.05374 [hep-ph]` (cit. on p. 50).

Appendices

A Oscillograms for energy independent decoherence

Oscillograms for different initial and final flavors using both standard oscillations and decoherence models with no energy dependence.

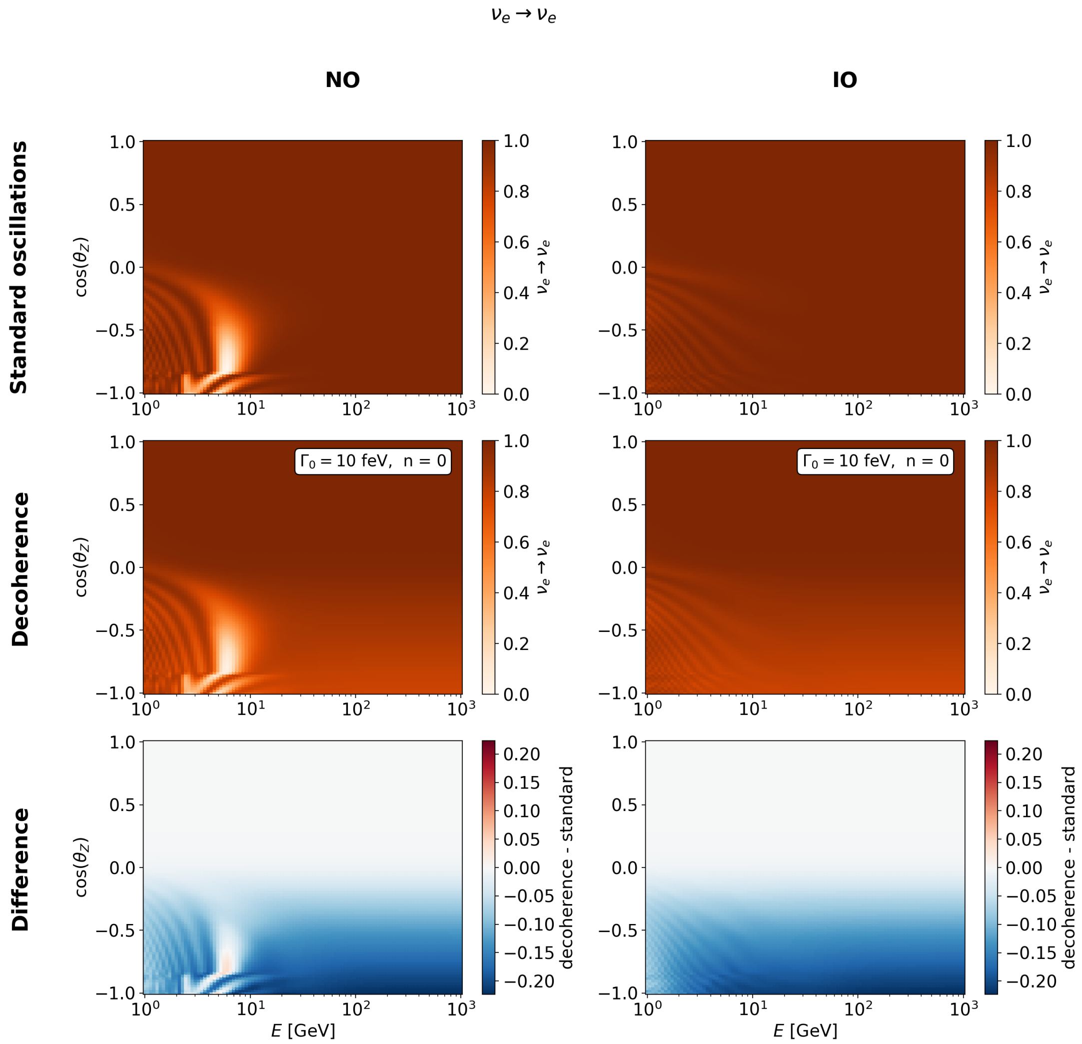

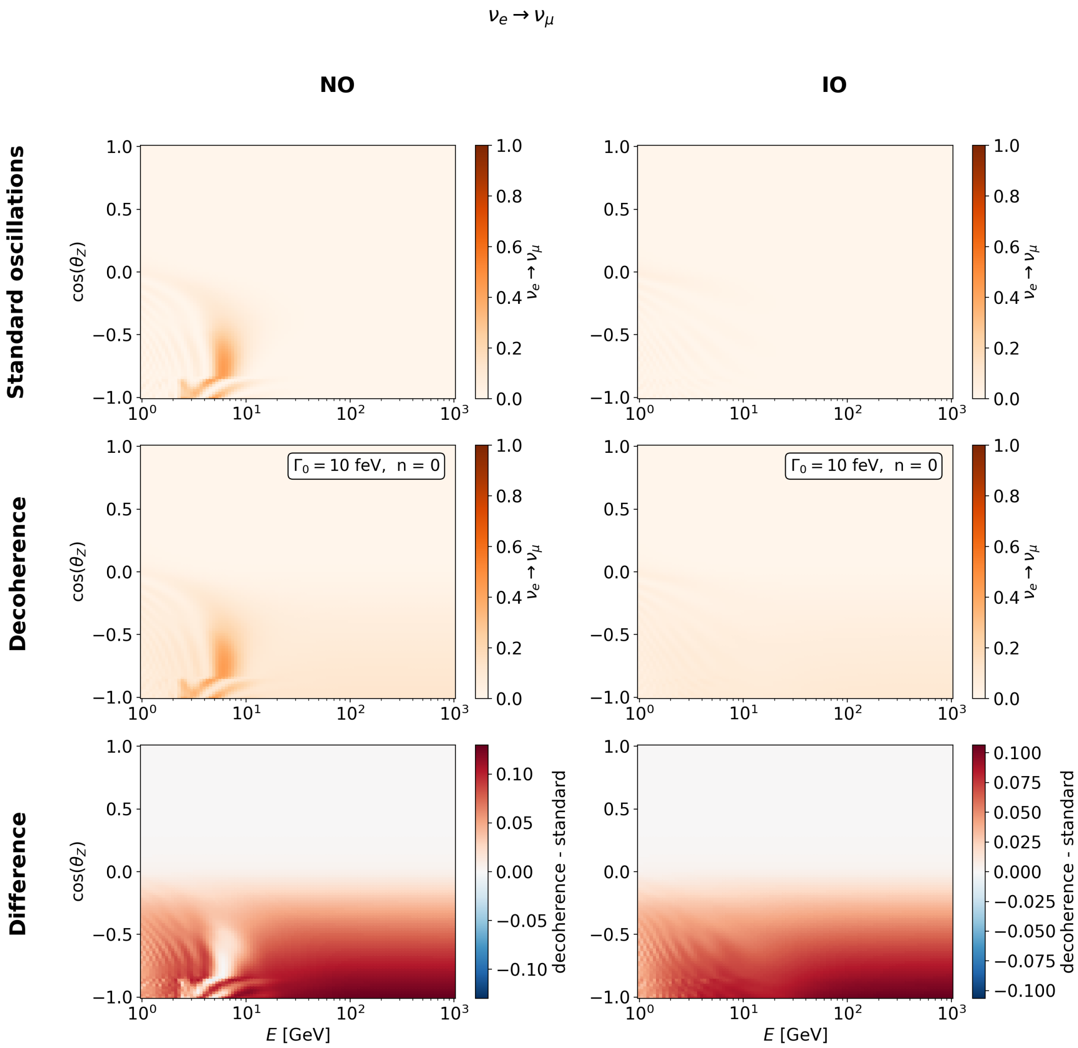
$\nu_e \to \nu_\mu$
NO
IO
Standard oscillations
Decoherence
Difference
$\cos(\theta_Z)$
$\nu_e \to \nu_\mu$
$\Gamma_0 = 10$ feV, n = 0
decoherence - standard
E [GeV]

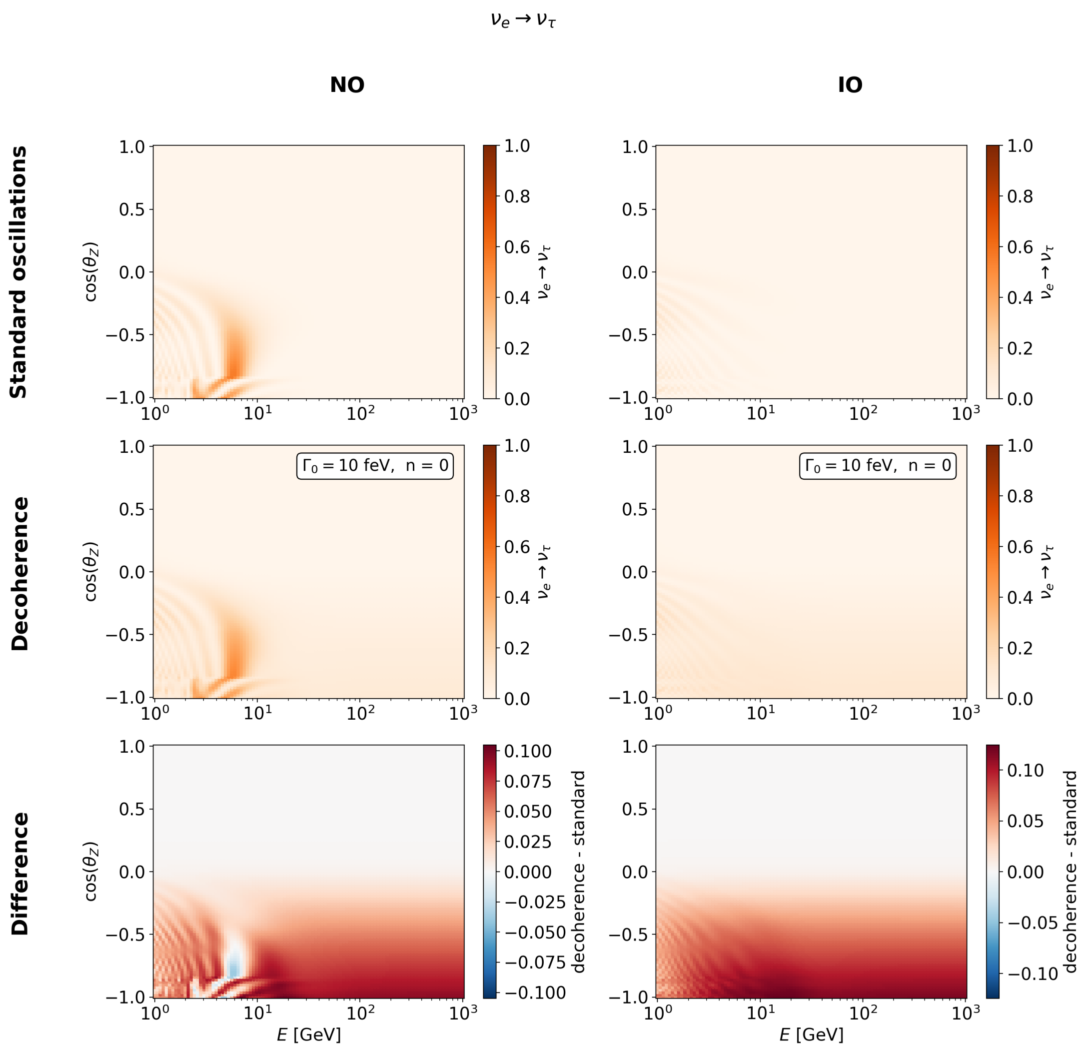
$\nu_e \to \nu_\tau$
NO
IO
Standard oscillations
Decoherence
Difference
$\cos(\theta_Z)$
$\Gamma_0 = 10$ feV, n = 0
$\nu_e \to \nu_\tau$
decoherence - standard
E [GeV]

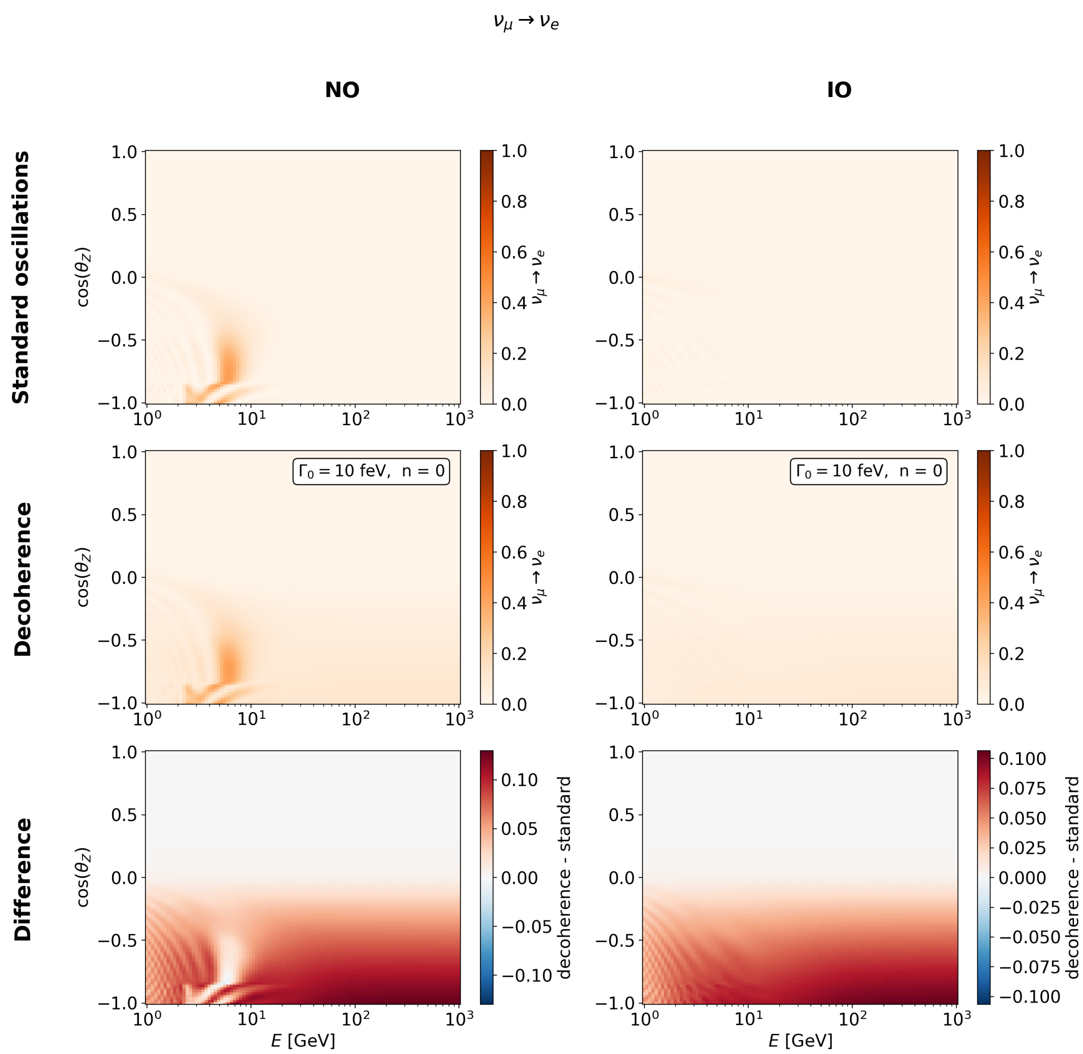

$\nu_\mu \to \nu_e$
NO
IO
Standard oscillations
Decoherence
Difference
$\cos(\theta_Z)$
$\nu_\mu \to \nu_e$
$\Gamma_0 = 10$ feV, n = 0
decoherence - standard
E [GeV]

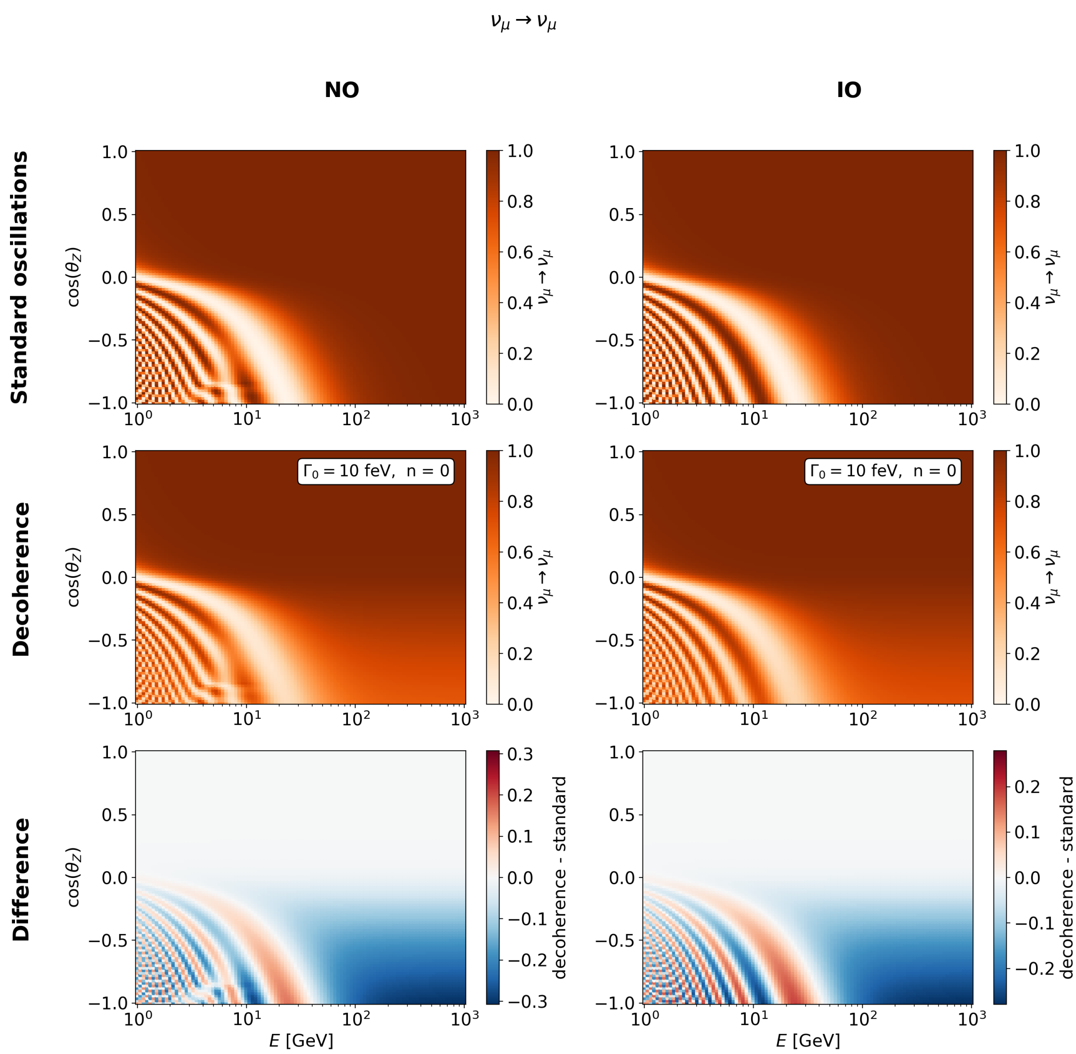
$\nu_\mu \rightarrow \nu_\mu$
NO
IO
Standard oscillations
Decoherence
Difference
$\Gamma_0 = 10$ feV, n = 0
$\cos(\theta_Z)$
$\nu_\mu \rightarrow \nu_\mu$
decoherence - standard
E [GeV]

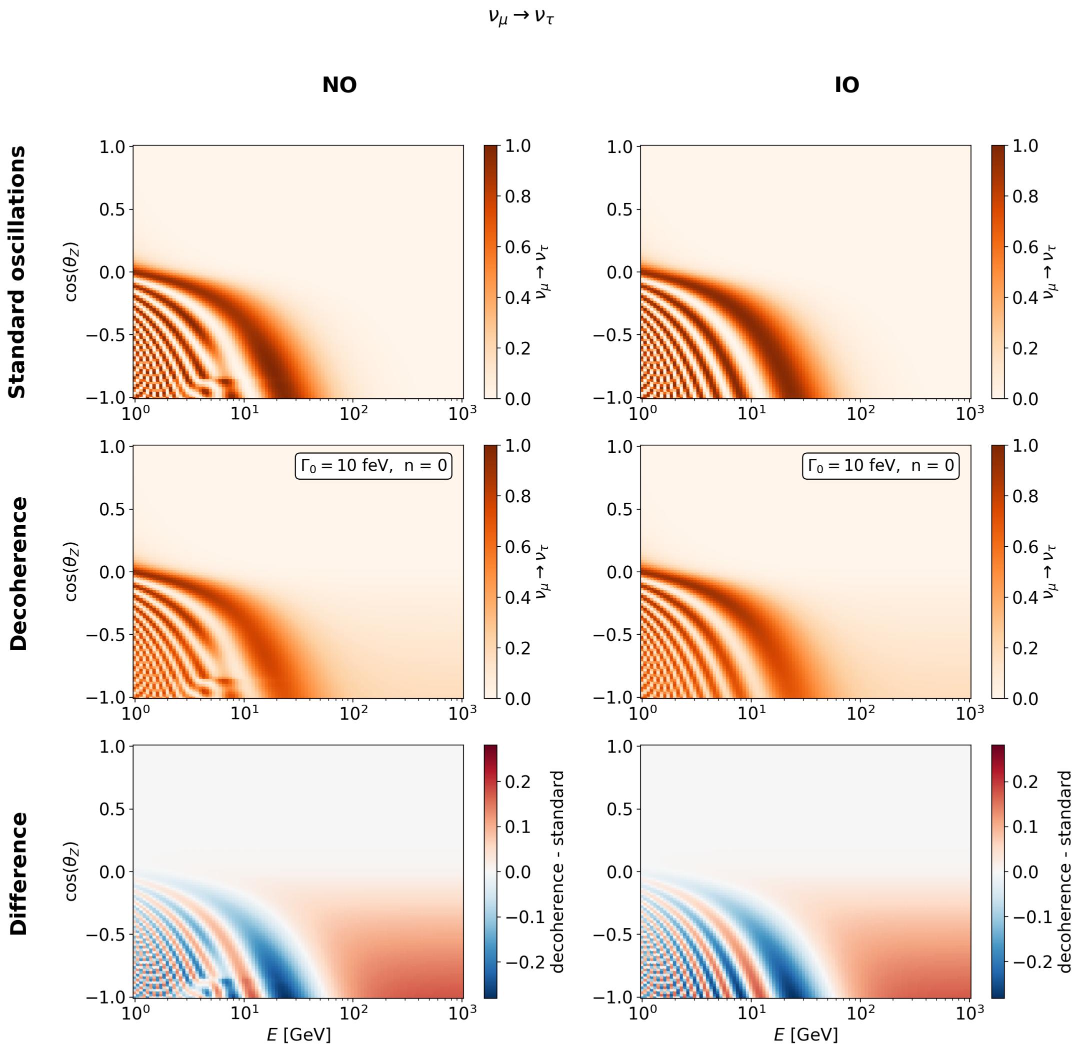
$\nu_\mu \rightarrow \nu_\tau$
NO
IO
Standard oscillations
Decoherence
Difference
$\cos(\theta_Z)$
E [GeV]
$\Gamma_0 = 10$ feV, n = 0
$\nu_\mu \rightarrow \nu_\tau$
decoherence - standard

B Templates and sensitivity for different energy dependences

B.1 n = -2

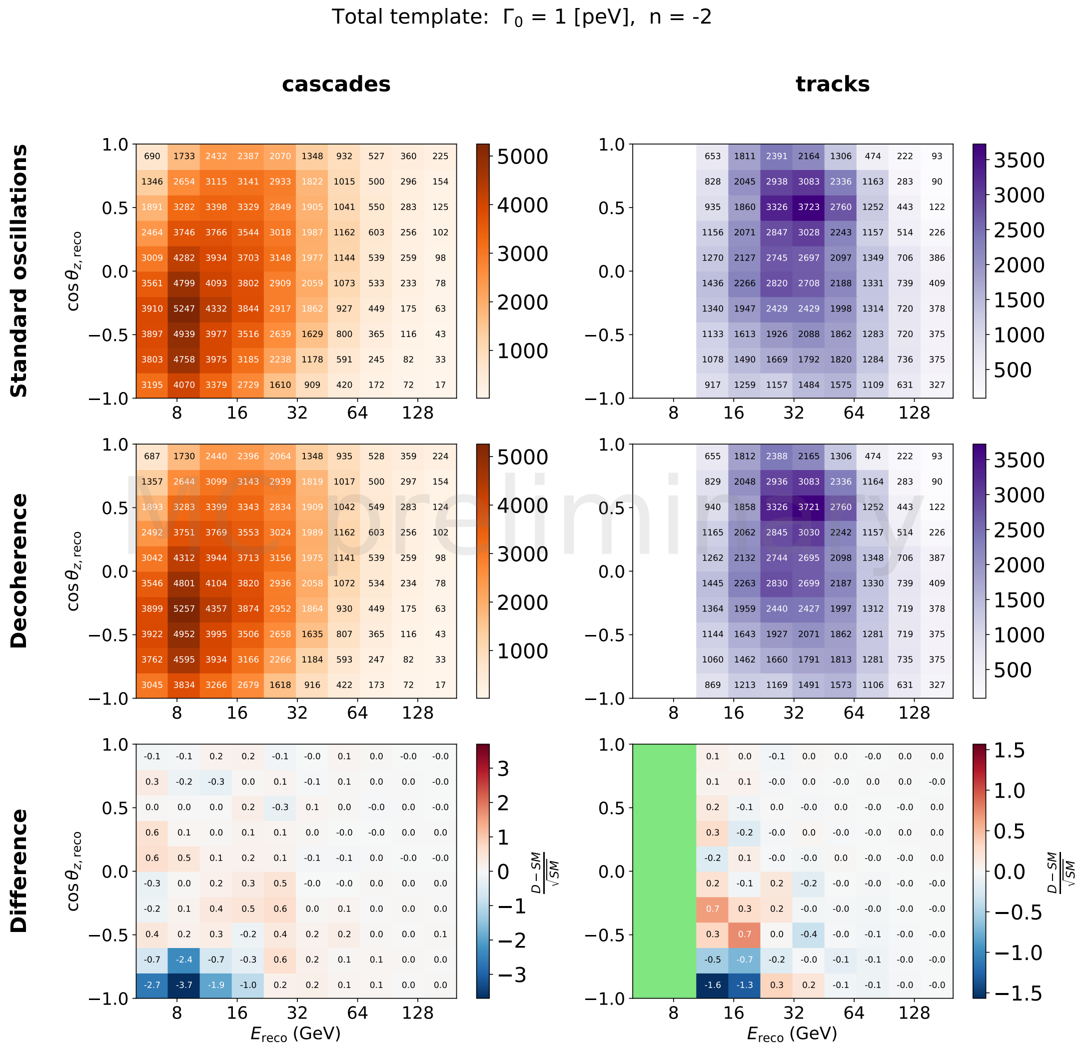

Figure B.1. – Number of events per bin as function of reconstructed energy and zenith angle. The decoherence model used is the single Γ model with $\Gamma_0 = 1 peV$, corresponding to the strength required for a 5σ discovery potential when using IceCube/DeepCore.

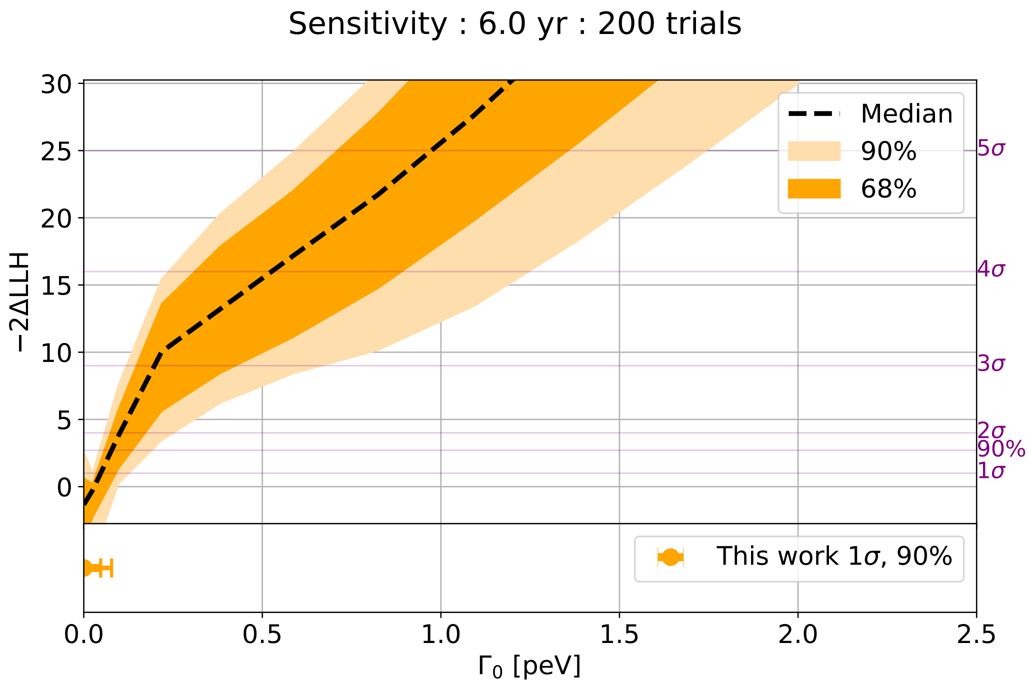

Figure B.2. – Sensitivity to decoherence using pseudodata generated with $\Gamma_0 = 0$ and $n = -2$. The confidence intervals are made by displaying the area that 68% and 90% of the trials fit within.

B.2 n = -1

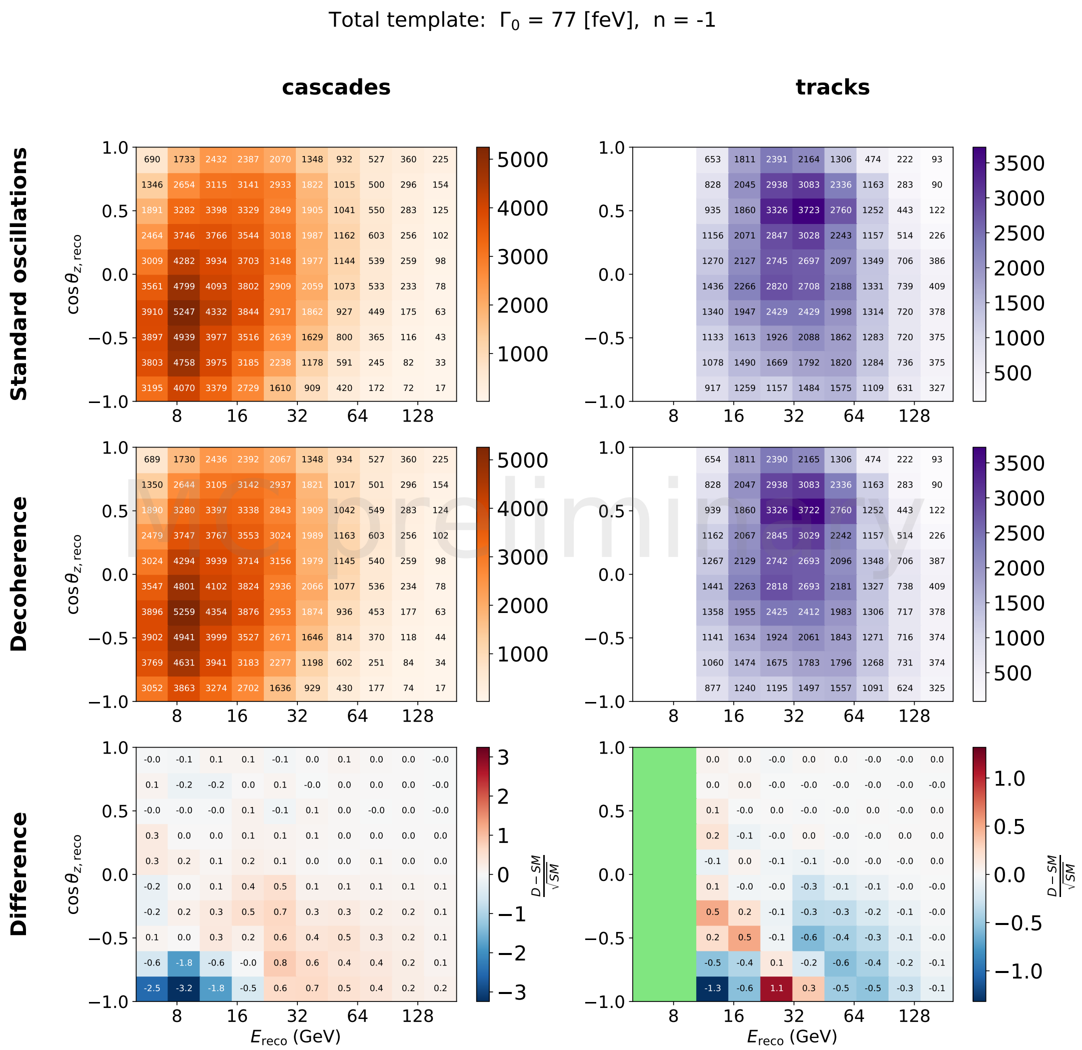

Figure B.3. – Number of events per bin as function of reconstructed energy and zenith angle. The decoherence model used is the single Γ model with $\Gamma_0 = 77 feV$, corresponding to the strength required for a 5σ discovery potential when using IceCube/DeepCore.

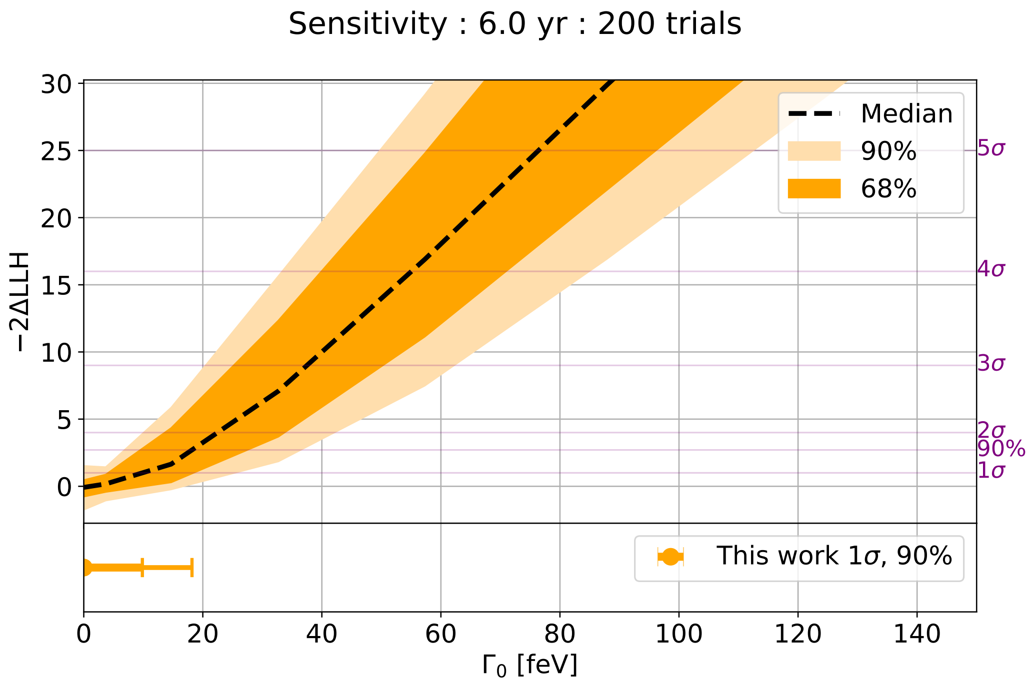

Figure B.4. – Sensitivity to decoherence using pseudodata generated with $\Gamma_0 = 0$ and $n = -1$. The confidence intervals are made by displaying the area that 68% and 90% of the trials fit within.

B.3 n = 1

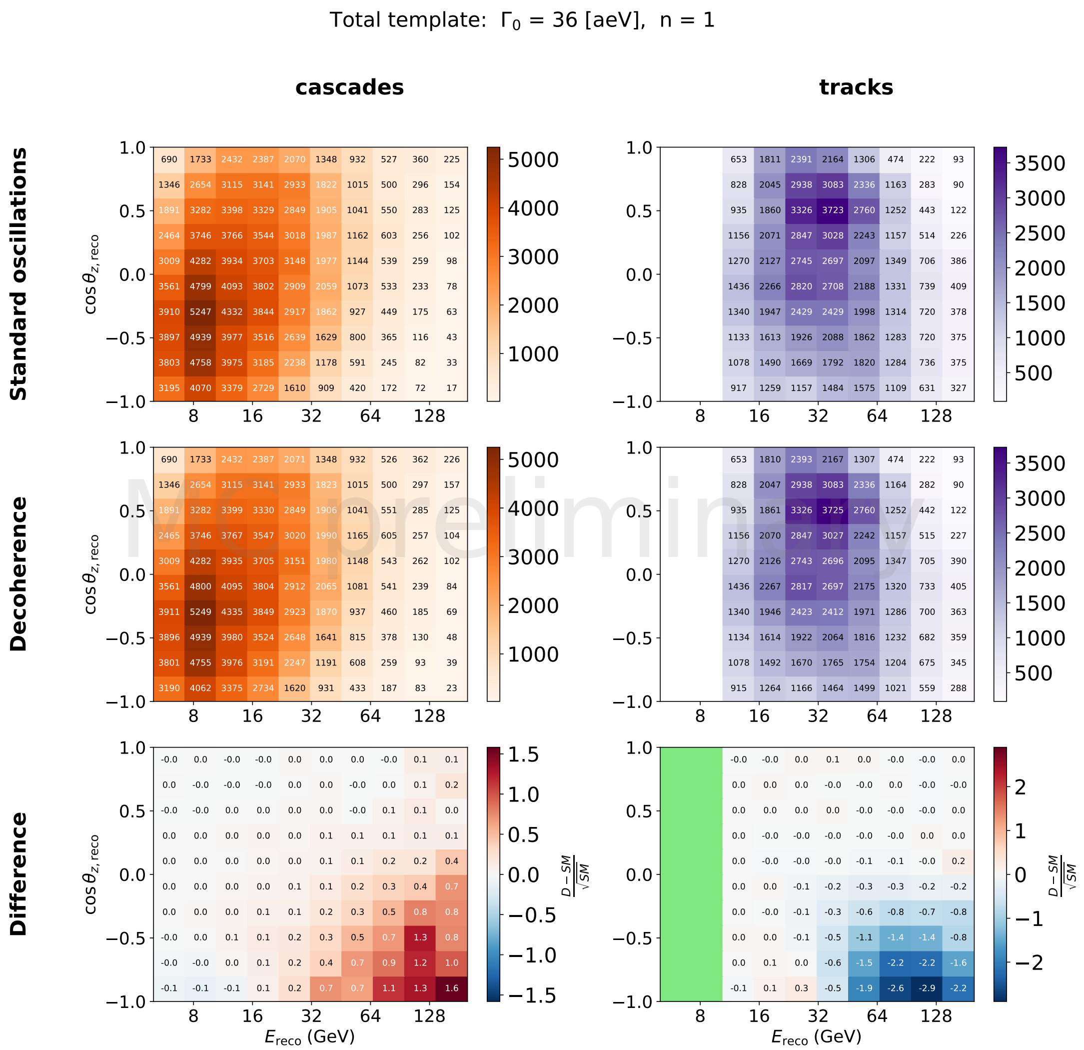

Figure B.5. – Number of events per bin as function of reconstructed energy and zenith angle. The decoherence model used is the single Γ model with $\Gamma_0 = 36aeV$, corresponding to the strength required for a 5σ discovery potential when using IceCube/DeepCore.

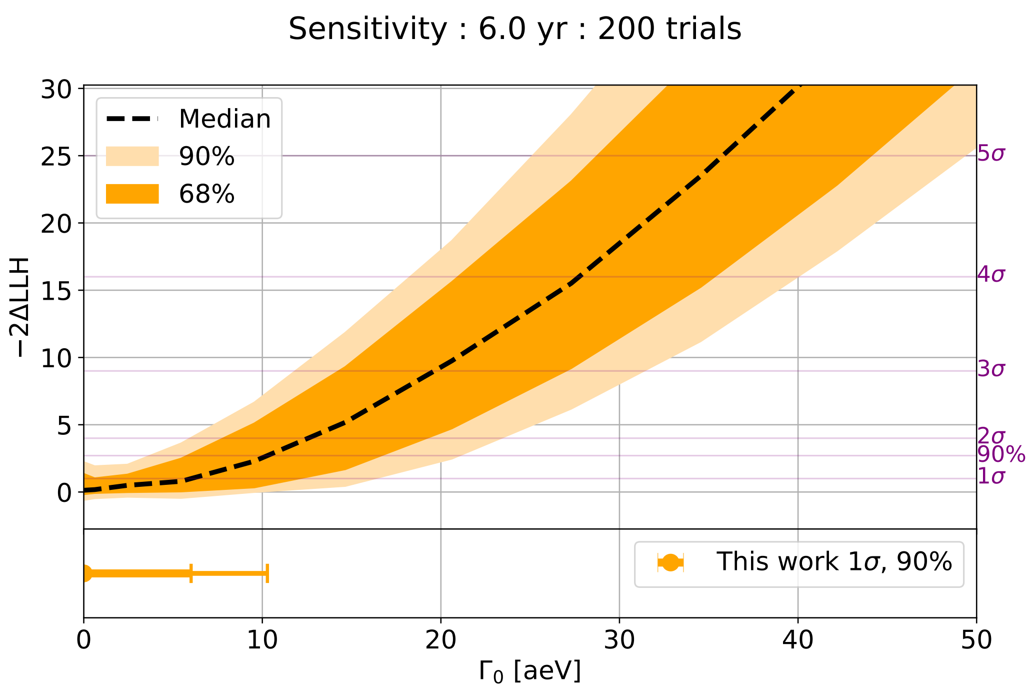

Figure B.6. – Sensitivity to decoherence using pseudodata generated with $\Gamma_0 = 0$ and $n = 1$. The confidence intervals are made by displaying the area that 68% and 90% of the trials fit within.